DESIGN AND APPLICATION OF HOLLOW SILICA MICROSPHERES FOR DENSITY-BASED BIOSEPARATIONS

by

Lichen Xiang, B.S., M.S.

A dissertation submitted to the Graduate Council of
Texas State University in partial fulfillment
of the requirements for the degree of
Doctor of Philosophy
with a Major in Materials Science, Engineering, and Commercialization
December 2016

Committee Members:

Shannon E. Weigum, Chair

Tania Betancourt

Gary W. Beall

John C. Carrano

Yihong Chen

FAIR USE AND AUTHOR'S PERMISSION STATEMENT

Fair Use

Duplication Permission

ACKNOWLEDGEMENTS

There are a number of individuals whom I want to thank for their help and support throughout my Ph. D. study journey. First and foremost, I would like to thank my advisor Dr. Shannon E. Weigum with my deepest gratitude and respect. Dr. Weigum has provided support for me in every aspects of my life, sometimes her help and encouragement are way beyond a duty of an advisor needs. Her personality and working philosophies truly impressed and influenced me deeply, which has helped and directed me to grow as a scientist and a good man. I would also like to express my committee members, Dr. Yihong Chen, Dr. Gary Beall, Dr. Tania Betancourt, and Dr. John Carrano, for their valuable insight and advices that helped to this dissertation work.

Furthermore, I will thank for Dr. Gabriel P. López, and his Ph.D. student Linying Li from Duke University for their assistance and guidance of this project. To the entire Dr. Weigum group, past and present, with particular thanks to Preethi Vaidyanathan for her kindest assistance for guiding me initialize my research. To Zhenyuan Lu for helping me take and edit video shots and photographs. To Kshitij Ranjan for discussing problems when I have doubt in my research. To Erica G Osta for her hard work as my assistant. To all of the members in Dr. Qiangkai Yu and Dr. Yihong Chen's lab that worked with me through tough times.

I want to thank the entire Materials Science, Engineering, and Commercialization program at Texas State University for giving me this tremendous opportunity to study and do research with such an elite team. Every single professor and staff in this program gave me uncountable help. I would also like to extend my gratitude to the National Science Foundation (NSF) Partnership for Research and Education in Materials, NSF's Research Triangle MRSEC and PREM for funding my project.

My deeps thanks to my mother, my father, my grandparents, and my entire family. It was their endless support pushed me through all of the troubles and difficulties. I would

also like to express my guiltiness for studying aboard, so that I was not able to take care of them for over 6 years. I will always love you all until the last minute of my life.

A special thanks to my girlfriend Tingting Iwasaki, who has more patience and love for me then I often deserve. Her kindness, support, encouragement, and love always motivate me to achieve more than I ever believe I could.

Again, thanks to all my teachers, friends, coworkers, and families with my deepest gratitude!

TABLE OF CONTENTS

Page

LIST OF TABLES

Table **Page**

LIST OF FIGURES

Figure **Page**

ABSTRACT

Challenges to the detection of low-abundance biological analytes from complex mixtures, such as biological fluids and food extracts, still exist and are critical for the management of infectious diseases like influenza and gastroenteritis. Typically, analytes must be separated and concentrated from complex sample matrices in order to meet the sensitivity and purity requirements of the downstream detection system. Unfortunately, many of the existing separation methods are time consuming and/or costly, which limits their use in point-of-care settings, such as a rural clinic or doctor's office in developing countries, where rapid diagnostic testing is vital to initiating treatment. The goal of this dissertation work was to develop a bioseparation approach that is inexpensive and easy to use, with absolutely no external instrumentation required. Our "molecular buoy" approach used low-density hollow silica microspheres, functionalized with target-specific antibodies to bind and separate target biomolecules from a complex sample matrix by floatation. We characterized the size and floatation properties of the hollow microspheres in aqueous solutions of increasing density and viscosity. Separation times were found to be inversely proportional to the microsphere size and directly proportional to the solution viscosity. Methods for surface functionalization with protein G were established with an estimated binding capacity of 31 µg/mg for size-fractionated microspheres 38 µm in diameter, and 50 µg/mg for size-fractionated microspheres 81 µm in diameter. We then applied the molecular buoy bioseparation method to the isolation of an infectious disease pathogen *Cryptosporidium parvum*, a protozoan parasite that is a common cause of acute/persistent diarrheal illness. When spiked into buffer or watery stool at known *C. parvum* oocyst concentrations, we obtained a relatively high capture efficiency (average recovery rate 95.4%) in less than 5 minutes. In addition, we integrated this novel buoyancy-assisted separation approach with a colorimetric paper-based microfluidic test to ultimately demonstrate a low-cost and instrumentation-free method that sequentially achieves complete sample-to-answer diagnostics. It is expected that this research will establish new

materials and methodologies for rapid bioseparation from complex matrices that are applicable to diverse protein analytes, biomarkers, and pathogens for improved detection and bioanalysis of infectious diseases.

I. INTRODUCTION TO BIOSEPARATIONS

1.1. Overview

In recent decades, bioanalytical technologies and instruments have improved dramatically in terms of the analytical accuracy, ease for operation, and multi-tasking capability. However challenges remain to detect and quantify low-abundance biomolecules in the presence of complex mixtures, such as biological fluids, food extracts, or other environmental composites [1, 2]. Therefore, isolation, separation, and purification of biological analytes from complex fluids are routinely applied prior to biological target analysis, especially in the pharmaceutical and medical field [2-6]. Biological analytes, such as proteins, nucleic acids, living parasites, toxic chemical matters, and drugs in body fluids are usually purified, concentrated, and isolated from the complex biological fluid, to meet the detection parameters of downstream analysis, via gas chromatography (GC), high-performance liquid chromatography (HPLC) mass spectrometry (MS), Nuclear magnetic resonance (NMR), UV-detection, and optical observations, or other methods [7-9]. Different separation mechanisms and methods are based upon the unique properties of the biological analytes, such as solubility, electronic charge, particle size, or other affinity interactions [10]. In addition, the separation method must also meet the requirements of their downstream analysis. For example, the needs of the total amount of the recovered analytes, biological activities of recovered analytes, and purity of recovered analytes will be the important factors for choosing the best fit separation methods [10]. The detailed separation mechanisms and the common bioseparation methodologies will be discussed below.

1.2. Existing bioseparation methods

1.2.1. Precipitation

Biological materials have their own unique structures and properties. Different kinds of proteins differ in the amino acids that locate at their surfaces, which results in the different charges, polarities, and hydrophobicity. Therefore, different proteins appear unique in solubility in particular sets of conditions. When some additives, such as neutral salts or organic solvents, are present in the protein solution, the particular protein will tend to precipitate differently from the solution, and this provides a pathway to separate. In practice, fractional precipitation is one of the most popular bulk separation methods, by controlling the solvent composition or pH. The introduction of high concentrations of salts to protein solutions will lead proteins to precipitate by removing water of solvation from their hydrophobic backbones, and result in allowing these hydrophobic backbones to interact with each other with resulting aggregation [10]. Under the assumption of pure protein solution, the protein solubility (S, in unit of g/kg of water) and the ionic strength (I, in unit of mol/kg of water) have an exponential relationship by:

$$\boldsymbol{logS = \beta - K_s[(I/2)]} \quad \textbf{[}\text{Equation 1]}$$

Where β and K_s are constants for particular protein at fixed pH and temperature [11, 12]. A variety of salts have been used for controlling protein solution pH for fractional precipitation, including NaCl, Na_2SO_4, KCl, $CaCl_2$ and $MgSO_4$, but the most commonly used salt for protein precipitation is ammonium sulfate $(NH_4)_2SO_4$. It is because the density of saturated ammonium sulfate (1.235g/ml) is lower than that of protein, which allows the precipitated protein to be collected by centrifuge easily, without physical damage. Other than salt, proteins can also be precipitated by introducing organic solvents, such as acetone and ethyl alcohol; however, the organic solvent can potentially cause protein denaturation

by interaction between solvent and proteins' hydrophobic residues [13]. The problem of the fractional precipitation method, in general, is that different kinds of proteins may have overlapped precipitation pH ranges, therefore, it is not possible to separate a specific protein from a complex protein mixture with high purity, by using the fractional precipitation method alone. For large-scale separation, the fractional precipitation method is a common procedure that is used at early-stage of purification and separations [10].

1.2.2. Ion Exchange

Ion-exchange chromatography is one of the most widely used methods to separate biomaterials via their net electronic charge. Ion-exchange chromatography relies on the interaction between charged molecules in sample/buffer solution (mobile phase) and oppositely charged packing matrix (stationary phase). The total net charge of a protein is dependent upon the combination of both positively and negatively charged amino acids. The net charges of these amino acids could exhibit differently, by varying the buffer acidity (hydrogen ion concentration). The more acidic the solution (lower pH), the more groups will be protonated, and exist positively charged; in contrast, the more alkaline solution (higher pH), deprotonated side groups will make the protein exhibit negatively charged [10]. The binding and elution of proteins are based on the competition between counter charged ions in the buffer and stationary phase to the charged proteins. The higher the concentration of salt in buffer, the greater competition for binding interaction to the stationary phase. At a low salt concentration condition, charged groups on proteins have greater affinities to interact with column. So, to provide better column binding interactions, the binding buffers are usually less concentrated with salt. For the purpose of elution, the

interaction of protein and buffer is required to be greater than the binding strength between proteins and column, thus, a high salt concentration buffer will be preferred [14].

The stationary phase of ion exchange chromatography can use swollen loose beads, dry granular materials, or some commercially available pre-packed columns, such as monolithic columns, and ion exchange membranes. The ion exchanger groups on the stationary phase can be categorized via charge types and binding strength. The common stationary phase exchanger groups are listed in Table 1. The stationary phase type is also dependent on the resolution requirements and sample quantities. For example, in a large-scaled separation scenario, fibrous cellulose-based resin will be preferred, due to its good flow rate with large bed volume, but it cannot provide a high resolution isolation. A high resolution separation can be pursued by using sepharose-based materials, however, it should be used in small-scaled samples.

Table 1. Category of commonly used ion exchange groups for ion-exchange chromatography stationary phase materials.

Ion exchange type	Strong exchangers	Week exchangers
cation	Sulfoprpoyl (SP)	Carboxymethyl (CM)
	Methyl sulfonate (MS)	
anion	Quaternary ammonium (Q)	Diethylaminoethyl (DEAE)
	Quaternary aminoethyl (QAE)	

Some other optimized ion exchange separation methods are also available, such as ion exchange ultrafiltration, chromatofocusing approach, and isoelectric focusing method. Similar to ion exchange chromatography, the ultrafiltration method uses ionized membrane assistance with pressure to separate charged biomolecules, the detailed mechanism will be discussed in the following section. The chromatofocusing separation method is an optimized ion exchange chromatography system, but instead of regular elution buffer, this

method is to gradually control the elution pH to reach the isoelectric point (net charge equal 0) to elute proteins from the column [15]. The isoelectric focusing method is a type of electrophoresis method, by utilizing pH gradient in an electric field to make charged samples migrate toward to the anode or cathode [16].

In general, ion exchange chromatography is a very powerful and efficient way to separate biomolecules via their net charge properties. It can be applied to either large-scaled or small-scaled separation conditions. The resolution of the separation can also be easily controlled by switching buffers and columns. In the meanwhile, ion exchange chromatography has some disadvantages as well. Since the elution efficiency is based on the competition between elution buffer and column, the greater salt concentration of elution buffer will be used for strongly binding of proteins ions and column ion exchangers. It turns out that high concentrated salt buffer may potentially influence the protein activities. It is also noticeable that some of the proteins may have similar ranges of net charge at a particular pH, but differ at another, therefore, common ion exchange chromatography procedures include multiple ion exchange steps either by using the same stationary phase but different pH buffers, or same buffer composition but a different column. This will cause the concern of over consumption of the operational time and materials, in addition, the quantity and quality of recovered proteins.

1.2.3. Size exclusion chromatography and micro- or ultrafiltration

Biological separation via the property of molecular size is one of the most direct and simple ways to achieve the goal of analyte isolation. Size-exclusion chromatography and ultrafiltration are two common methods to separate biological substance. In traditional

size-exclusion chromatography and ultrafiltration, sample solution is passed through a porous column, and the pores sizes must not allow large-sized molecules to access, small sized molecules have free access to those pores, and intermediate-sized ones have partial access to small pores. Thus, the large molecules will have the shortest retention time in the column because of the shortest pathway. On the other side, the small molecules will elute last because of the longer pathway for travelling through the column.

In biological separation, size-exclusion chromatography exhibits limited resolving power, due to the size similarity between target analytes and other biomolecules in a complex biofluid. However, it is a very useful method to separate biomolecules with large difference in size, such as protein aggregation removal, DNA or virus removal from protein samples, buffer desalting, or study of protein folding [17-20]. Another disadvantage of size-exclusion chromatography is its low capacity, because the volume of buffer solution is required to be as small as possible for the resolution needs [10].

Ultrafiltration involves forcing a sample solution through membrane with pores of controlled sizes and shape. In some applications, ion exchanger modified membranes are utilized to separate charged biomolecules. Since the ultrafiltration process is required to employ a low-pressure force to lead the sample solutions to pass through the membrane, centrifugal force is one of the best choices. The centrifugal ultrafilters have a wide range in volume capacity from 0.5 to 30 ml. The normal spinning time at room temperature is 5 to 60 minutes [21]. Ultrafiltration separation method can be categorized as reverse osmosis or microfiltration based on the different membrane types and filtration methods. Reverse osmosis is usually applied to separate low molecular weight molecules (normally less than 100 Daltons) [22]. Microfiltration uses the traditional porous membranes with pore sizes

in the micron range (0.2 μm to 5μm). This microfiltration process is able to retain bacteria, colloids, and micron-sized particles [23].

In summary, ultrafiltration is an efficient way for laboratory biological separation with a low risk of denaturation of sample. This method is widely used to concentrate samples, remove non-bioparticle-bound substances, recovery from electrophoresis gels, or other biological purification applications. It is relatively a low cost and less time consuming method. But in the case of large-scaled separation, centrifuge, pumps, or other devices are required for applying force to transport samples to pass the membranes, it limited the potential of applying this method to field-based point-of-care (POC) applications. For devices that do not require additional instrumentation, such as capillary-drivendevices, they will be able to isolate only small, or very dilute samples. Another shortage for ultrafiltration are the solute-solvent or solute-solute interactions. For example, if polymerization reaction, hydrophobic aggregation, or other potential reactions occur in the middle of filtration, at certain concentration and/or buffer conditions, the morphology and other properties of the targeting analytes will change to cause problems of the permeation and retention [10, 22-24].

1.2.4. Affinity purification

1.2.4.1 Affinity chromatography

Affinity interactions, such as hydrogen bond, electrostatic interaction, hydrophobicity interaction, or Van der Waals interactions, often occur between biomolecules with a high selectivity, for instance, antibodies specifically bind to antigens, enzymes bind to activators, inhibitors and targeting substrates, and hormones bind to

receptors. All of these interactions can be exploited to isolate target analytes by immobilizing the biospecific ligand to a substrate or support (normally in the solid phase). Then, analytes contained in a mixture will be passed through, or incubated with the pre-functionalized substrate. Only target analytes will bind with the immobilized ligands via specific binding interactions, while all other materials will remain in the mobile phase and are washed away. The elution process is normally achieved by either introducing a new targeting molecule that has stronger affinity to the ligand or analyte, or controlling the buffer conditions to deactivate protein-analyte binding [10, 25]. The schematic demonstration of general affinity process is showed in Figure 1.

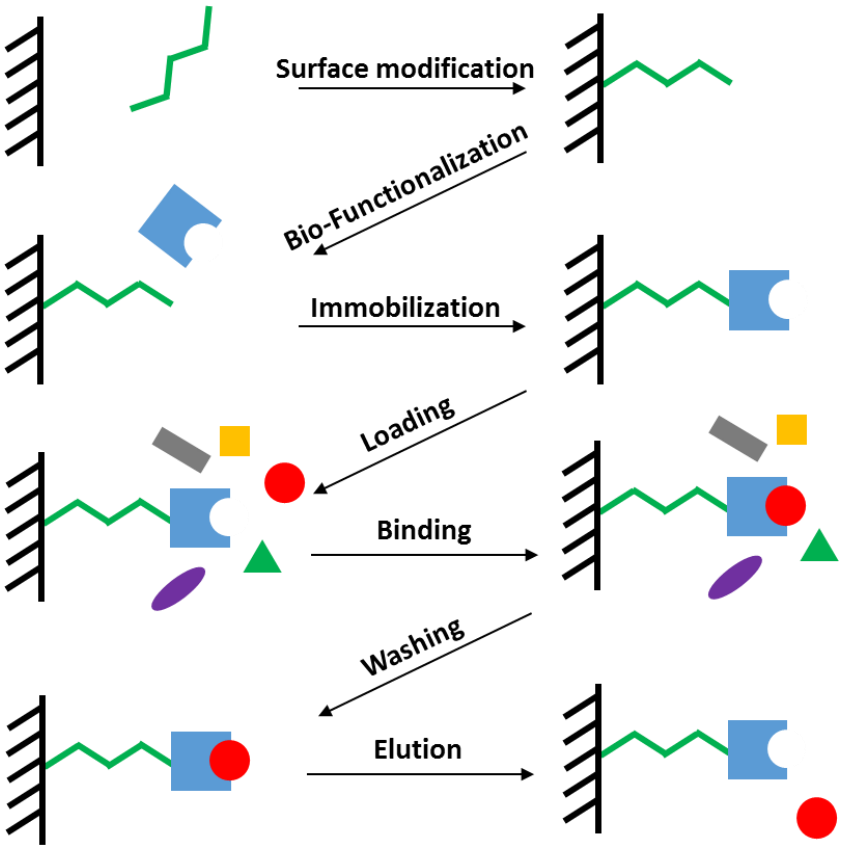

Figure 1. Principle of affinity biological separation.

The separation method via specific binding force is generally called affinity chromatography. The ligands in affinity matrices can be either mono-specific or group-specific. Mono-specific affinity ligands only recognize a single type of target biomolecules. For instance, an enzyme recognizing an inhibitor, a monoclonal antibody could only bind with one specific antigen, and a receptor has affinity to a particular hormone. Group-specific ligands, such as protein A, protein G, enzyme cofactors, and plant lectins, are able to bind a variety of targeting samples [10, 26, 27]. The commonly used group-specific affinity ligands and their targeting molecules are listed in Table 2, where the protein A and protein G are both able to bind IgGs, but they have differences in binding affinities between different species and immunoglobulin types (Table 3.). Both mono-specific ligands and group-specific ligands are widely used in the bioseparation industry for their unique purposes. Due to the unique feature of group-specific ligands, they are usually used for isolating different biomolecules that have similar functional groups or binding affinities. For example, if NAD cofactors are used as an affinity matrix, all kinds of dehydrogenases will be isolated, which is independent with their particle size, charge, and other physical properties.

Table 2. Some commonly applied group-specific affinity ligands

Ligand	Target particles
5' AMP, ATP	Dehydrogenases
NAD, NADP	Dehydrogenases
Protein A	Antibodies
Protein G	Antibodies
Lectins	Polysaccharides, glycoproteins
Histones	DNA
Heparin	Lipoproteins, DNA, RNA
Gelatin	Fibronectin
Lysine	rRNA, dsDNA, plasminogen
Arginine	Fibronectin
Benzamidine	Seine proteases
Polymyxin	Endotoxins
Calmodulin	Kinases
Cibacron blue	Kinases, phosphatases, dehydrogenases, albumin

Table 3. Binding affinities for protein A and protein G in different species and antibody types

Species	Immunoglobulin	Protein A	Protein G
Human	Normal IgG	++++	++++
	IgG1	++++	++++
	IgG2	++++	++++
	IgG3	-	++++
	IgG4	++++	++++
Mouse	IgG1	+	++++
	IgG2a	++++	++++
	IgG2b	+++	+++
	IgG3	++	+++
Goat	IgG	+/-	++
Rabbit	IgG	++++	+++

Mono-specific ligands have significant selectivity to their targeting molecules. Monoclonal antibody-antigen affinity separation is one of the most widely used methods to isolate particular antigens from biological complex fluid, due to its excellent selectivity. Thanks to the development of hybridoma technology, it is possible to generate economically viable amounts of monoclonal antibodies for the separation applications [28-

30]. Nucleic acid based ligands are also widely used as a high selective mono-specific type ligand. The natural DNAs, RNAs, or artificial DNA oligomers have specific sequence tags, which will bind with targeting molecules that contain the particularly matched tags [10, 31]. Moreover, streptavidin-biotin interactions, enzyme-based interactions, metallic specific interactions, or some dye-based biological interactions are also widely use as powerful biological isolation mono-specific ligands [10, 27, 32, 33].

As mentioned above, the affinity biological separation process begins with immobilization of highly selective ligands onto a solid substrate (Figure 1). Thus, the surface functionalization and biomolecule immobilization will be critical steps to influence the separation efficiency. The typical methodology for ligands immobilization is to modify the substrate surfaces to obtain uniform distributed functional groups. These functional groups will be then exploited to immobilize ligands via direct binding of the side-chain residues of antibodies and enzyme, such as amines, sulfhydryls, carboxylic acids, or the termini of nucleic acids and antibodies, which contain hydroxyl, amines, and carboxylic acids [10].

The elution process of affinity separation method is always a significant challenge. The principle to elute analytes from ligands are either by weakening the ligand-analyte interaction via change in pH, ionic strength, et al., or by adding specific particles that have stronger binding affinities to either ligand or analytes, such as a competing ligands [10, 26]. The eluents that are commonly used for the affinity separation process are listed in Table 4. It is important to note that most of the eluents involve changing the solution condition to an extreme level. This extreme elution condition will hardly retain the

functional and structural integrity of both the ligands and analytes [34]. Thus, to explore an efficient and gentle way to elute analyte is still a goal for researchers to pursue.

Table 4. Commonly used eluent for affinity separation and their principles.

Class of eluent	Principle
Glycine-NaOH, diethylamine, NH_4OH	High pH
Glycine-HCl, citric acid, HCl, Propionic acid	Low pH
Ethylene glycol, DMSO, acetonitrile, dioxane	Organic solvent
Tris-HCl, NaCl	High ionic strength
Deionized water	Low ionic strength
Guanidine HCl, Urea	Denaturant
KCl, KI, $MgCl_2$, NH_4SCN	Chaotropes

1.2.4.2. Magnetic nanoparticle separation

Recently, magnetic nanoparticle bioseparation techniques have become increasingly popular and widely applied in practical separation procedures [35]. The magnetic nanoparticle separation method uses magnetic nanoparticles (MNP) as the solid phase substrate. Typically, MNP is a spherical nano-scaled particle that contains a magnetic core covered with a protective polymer shell. This polymer shell is not only protecting magnetic core structures against the degradation and unexpected aggregation, but also provides functional groups, such as $–NH_2$, -COOH, -OH, and -SH, that enable to bind with biological ligands [36]. A schematic diagram of basic nanoparticle preparation and use in bioseparations is shown in Figure 2 [35]. Mostly, target-specific ligands, such as enzymes, oligonucleotides, or antibodies, are functionalized onto the MNP polymer shell via covalently binding interactions between functional groups on the shell and active functional groups on ligand particles. Those immobilized ligands provide unique selectivity to capture targeting analytes. Once the analytes are captured by immobilized ligands, the entire MNP complex can be isolated from the original liquid mixture by

applying an extra magnetic field, usually just simply by the use of a magnet [37, 38]. The isolated MNPs-analytes complex, can be further washed, the analyte will then be eluted for continuous downstream characterizations, while the eluted MNPs may or may not be re-used [38-41].

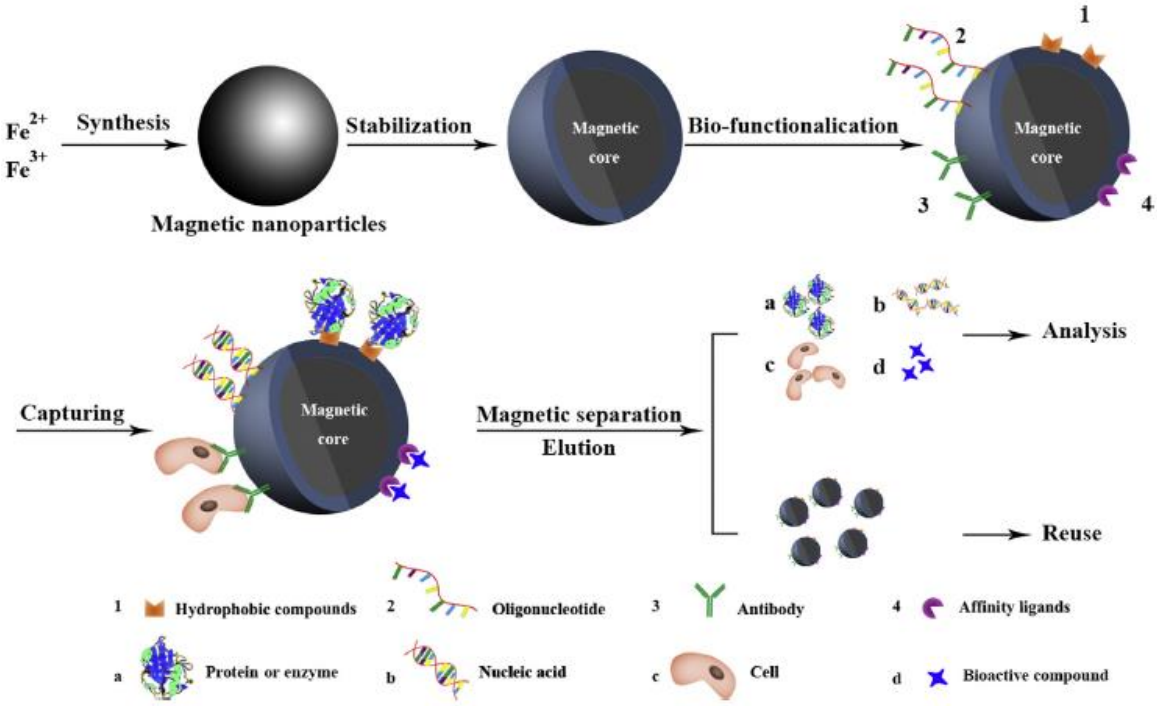

Figure 2. The general procedure of magnetic separation in sample preparation for biological analysis. Figure reprinted with permission from Elsevier, Journal of Pharmaceutical and Biomedical Analysis [35], copyright 2014.

To compare with other separation pathways that are discussed above, the MNP technique appears to have several unique advantages include: (i), MNPs have large surface area to be able to powerfully and efficiently separate either small or large scaled samples [42]; (ii), free of using additional hard process, which avoid to physically destroy and denature the biological analytes [43]; and (iii), analyte captured MNP-analytes complex can be isolated from the original sample solution easily and directly by using magnets or

applying an additional magnetic field [44]. However, commercially available magnetic nanoparticles are relatively expensive (~$5.50/mg), which greatly limits their application potentials for large-scaled consumptions or pair with low-cost disposable applications.

1.2.4.3. Automated cell sorting systems

Fluorescence activated cell sorting (FACS) and magnetic-activated cell sorting (MACS) are two common affinity-based sorting methods that have been fully automated to separate target analytes and whole cells. MACS uses magnetic tag, and the FACS uses fluorescent tags to separate cells [45]. For FACS cytometry, fluorescently labeled cells are delivered to a laser beam, detectors analyze the reflection of fluorescent light to control the gate, therefore, separate different types of cells [46]. MACS uses magnetic tag label the target cells, and separate cells by applying magnetic field externally. Cells that with magnetic tag will attracted by magnetic force, but others do not.[47] Both of the two methods provide highly specific separations, however, the throughput rate of them are not compatible with physical cell sorting methods, not even mention the labeling process of MACS and FACS are usually more time consuming. Another shortage of the MACS and FACS is the labeled tag need to be released from cells after separation. The de-tag process is not only increasing the complexity of the cell sorting, but also may cause the damage of the cell [48].

1.3. Emerging bioseparation methods

1.3.1. Microfluidics and Lab-on-a-chip systems for cell separation

Microfluidics is an interdisciplinary field connecting chemistry and engineering to build systems for fluid handling within micron-scale channels typically <100 μm in any width/height dimension [49]. The fluid volume that the microfluidic systems utilize could be as small as 10^{-9} to 10^{-18} L [50].

Like all kinds of traditional bioseparation methods, microfluidic cell separation can be generally split to two major categories based on their separation mechanism either be physical parameters, such as size, shape and density, or cell biochemistry based separations [50-52]. Inertial microfluidics is one of the most popular microfluidic techniques that use cell sizes and cell shapes to sort cells [53]. In the inertial microfluidic, two forces determine movement of cell in the channel, one is shear lift force, and the other is wall lift force[54]. The shear force drive the cell away from the center of the channel, and the wall lift forces particle away from the wall. Therefore, particles in different size and shape has their own inertial equilibrium and immigrate differently in the channel [55]. The inertial microfluidic cell sorting has a very high throughput at over 10^{10} cells/hour rate, which affinity based microfluidic technique can hardly meet [55]. Even though many inertial microfluidic techniques were reported to have an excellent separation resolution, it still limited by the requirement of distinguishable properties between the target and background cells [56].

In summary, existing microfluidics cell sorting techniques have their own pros and cons. New microfluidic system and optimizations of existing techniques are keep developing in this field. Lab-on-a-chip and microfluidics tend to be a trend to meet the need of modern bioanalytical as portable, low cost, and efficient [50].

1.3.2. Buoyancy-activated separation

A new bioseparation method called buoyancy-activated cell sorting (BACS) technique was recently reported by Hsu *et al.* in 2014 and Liou *et al.* in 2015 as an alternative approach to separate circulating tumor cells and cancer stem cells from whole blood [57-61]. BACS uses hollow microbubbles (1-30 μm in diameter) functionalized with target-specific ligands to actively bind or capture the target analytes and carry them to the top of the liquid, thus isolate the target analytes without using any additional instrumentations.

The low material cost is one of the major advantages of BACS over other separation methods, particularly magnetic nanoparticles. Besides, the nature of the floatation-based separation eliminates the need for external instrumentation like a centrifuge or magnet, which would not only reduce the overall cost of the separation, but also ease the separation process to make it possible to be used for portable laboratory or POC applications. Yet, some of the BACS still require a relatively long separation time to separate specific cells, which would obey the principle of rapid diagnostic for POC applications. In addition, the buoyancy-assist separation concept was neither reported to separate infectious diseases, nor integrate with POC diagnostic devices. Thus, to optimize the buoyancy-assist bioseparation concept to a low-cost, rapid, easy to use, and efficient separation tool for infectious illness, and further integrate with the low-cost diagnostic are needed.

1.4. Summary and dissertation overview

The preceding sections detailed the existing bioseparation methods. Each of these separation technique has its own advantages, yet they still have many disadvantages in

common include the high cost, long operation time, limited separation resolution, along with the need for highly skilled technicians, and the need for bulky instruments. Those disadvantages limit the capacity for traditional bioseparation method to integrate with portable, low-cost diagnostic POC detection systems and applications.

This dissertation focuses on developing a low-density hollow silica microsphere bioseparation platform that can be functionalized as biomolecule buoy carriers to separate target biomolecules from the sample matrix by floatation. The hollow silica microspheres are commercially applied for plastic material fillers or additives to decrease the materials densities but keep their strengths. The cost of the microsphere is a great advantage than any other commercially available bioseparation product, especially the MNP. The average cost of the raw MNP is around $5/mg beads (the cost analysis is depend on the average of five major magnetic beads suppliers), and the microspheres that we used is 0.01 cents per 1 mg. Besides, this method will also be a complex laboratory instrument free approach, which will greatly improve the cost efficiency and decrease the need of professional operation requirements.

The schematic of the hollow silica microsphere buoyancy-assist bioseparation concept for isolation of *Cryptosporidium*, a protozoan parasite that causes diarrheal illness is demonstrated in Figure 4. Microspheres were first functionalized with target-specific antibody, anti-*Cryptosporidium* mouse IgG, then incubated with *Cryptosporidium* contained stool sample. A constant mixing process was applied to facilitate the microspheres to capture the target pathogens. When mixing was stopped, the pathogen-bound microspheres move upward to the top of the solution by floatation, which separates and concentrates the target pathogens from the sample matrix without assistance from any

other instrumentation. As showed in Figure 4, inset, when the microfuge tube was tilted in an angel, the microsphere moved to the top corner of one side of the solution. The bottom fraction of the solution was easily removed by pipetting.

Cryptosporidium is a protozoan parasite that can cause diarrheal illness. Fecal floatation is a widely used method for the isolation and concentration of parasitic eggs and oocysts in stool for diarrhea diseases diagnosis in both human and animals traditionally [62-64]. The fecal floatation method is based on the gravity differences between the oocysts, stool debris, and the modified solution, where the parasitic eggs/oocysts that have the lowest specific gravity, and the stool debris have the highest [63]. Thus, the parasitic oocysts that have a lower density will float to the surface, in contrast, the debris will sink to the bottom after the centrifugation [63]. However, this separation has a low recovery rates, and it has to utilize centrifugation. In addition, the fecal floatation separation method could only be used as those organisms that have gas or air pockets to decrease their density, such as, eggs and encapsulated cysts. To overcome those disadvantages, the hollow silica microspheres will provide a density-based separation method that uses low-cost materials, without using any external instrumentations or even the centrifugation.

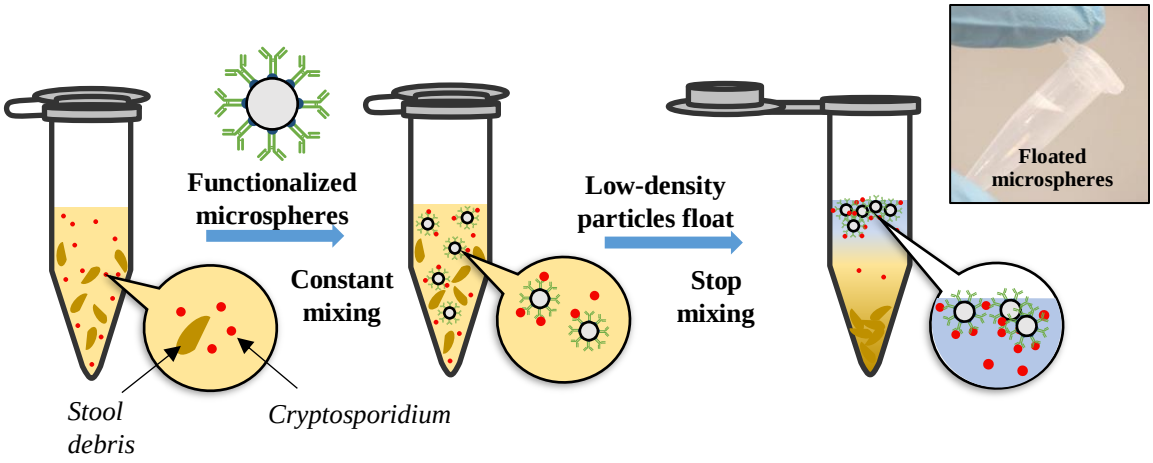

Figure 3. Schematic of the buoyancy-assist microsphere bioseparation concept for pathogen isolation in stool sample. The inner image is the photograph of microspheres float in BPS buffer in a microfuge tube.

The ultimate goal of this research is to integrate this hollow-microsphere-based sample preparation method onto a paper-based microfluidic platform that combines sample preparation with detection of pathogen bounded microspheres for a complete POC analysis system. The overall aims of this work are as follows: (1) To understand the properties of microspheres in terms of their physical properties that relate to their floatation kinetics. (2) To develop an efficient biofunctionalization protocol to immobilize the microspheres with the target-specific antibody. (3) To establish the efficiency and reproducibility of the isolation technique for *C. parvum* pathogens from a complex biological matrix such as stool. (4) To integrate the microsphere separation method with a paper-based diagnostic to ultimately achieve the goal of absolute instrumentation free and low-cost sample preparation and detection together. With the development of this new bioseparation technique, many of questions must be addressed in terms of the floatation properties of the microspheres, surface functionalization of the microspheres, capture efficiency of this

technique, design and structure of the paper-based diagnostic, and the limit of detection of the paper-based device. Points of focus for the dissertation include:

- What are the size of the microspheres and how does the size relate to their floatation properties?
- How long will the microspheres float from the bottom to the top in different solutions with different viscosities?
- How to functionalize microspheres with target-specific antibodies? And how to prevent non-specific binding?
- What is the binding capacity of the microspheres?
- Can antibody functionalized microspheres capture the target pathogen? If so, how efficiently can microspheres separate pathogens from a complex biological solution, such as stool?
- How to integrate microspheres with a paper-based device?
- How to quantify the amount of pathogens that are isolated by microspheres and what is the limit of detection of this technique?

This dissertation aims to develop the microspheres separation technique and apply it with the diagnostic device by solving the problems that are listed above. The following chapter details the physical properties characterization of the microspheres include the size of the microspheres, the floatation kinetics of different sized microspheres, and the floatation kinetics of microspheres in different solutions with different viscosities. Once the floatation properties of the microspheres were characterized, the examination of microspheres surface functionalization was necessary. Chapter 3 serves to optimize the conditions of functionalization of microspheres with target-specific antibodies. We used

an existing epoxy silane group on the microsphere surface to directly conjugate protein G to the microsphere via a pH-dependent ring-opening reaction [65]. A series of optimization tests were also conducted by changing the pH conditions and the concentration of the protein G to find the best functionalization conditions and the binding capacity of the microspheres. After we found a way to functionalize the microspheres with antibody, Chapter 4 presents the results for the *C. parvum* pathogen isolation from stool by using the microspheres. In addition, the separation efficiency of the microspheres were also investigated. A downstream paper-based diagnostic device was also designed and integrated with the microsphere separation method.

Collectively, the body of this dissertation seeks to establish new materials and methodologies for rapid bioseparation of infectious pathogens from complex matrices. And further develop a paper-based diagnostic device to integrate with the separation method to make the sample preparation plus diagnosis be rapid, reliable, and instrumentation free at the same time. Ultimately this research aims to apply this buoyancy-assist microsphere bioseparation method to be applicable to diverse protein analytes, biomarkers, and pathogens for improved detection and bioanalysis of infectious diseases.

II. CHARACTERIZATION OF FLOATATION PROPERTIES OF HOLLOW SILICA MICROSPHERES

2.1. Introduction

In the current chapter a series of physical property characterization of the microsphere are presented. As discussed in the previous chapter, when a spherical object submerge into a liquid, three forces that include the force of gravity, drag force (Stocks' law), and buoyancy force (Archimedes' law), dominate the movement of the object to be float upward, sink to the bottom, or suspend in the middle of the liquid. The buoyancy force of a fully submerged object equals to the mass gravity of the liquid that is displaced by the object, therefore, the buoyancy force is related to the volume of the object. So, the size of the microsphere is a major factor to affect the floatation kinetic. The larger of the object, the much volume of liquid can be displaced, thus the buoyancy force will be greater. On the other hand, as an opposite force to the buoyancy force, the drag force is a liquid viscosity related force to hinder the object to float upward. In order to understand the floatation property of the microsphere, the particle size and the viscosity of different liquid need to be tested. The study of the floatation property of microspheres is the fundamental of the development of this microsphere bioseparation technique, because the floatation efficiency is not only related to how rapid could the microsphere float, but also highly related to the separation efficiency of pathogens later on. Besides, the selection of a particular sized microspheres into specific applications are critical too. Utilizing wrong sized microspheres will cause either long separation time, or too fast to interact with pathogens in the biological matrix.

2.2. Experimental methods

2.2.1. Materials and reagents

The hollow silica microspheres used in this research are the H20 and H50 glass bubbles, with an epoxy silane surface treatment and a density of 0.2 g/cm^3 and 0.5 g/cm^3, respectively from 3M (H20/H50 glass bubbles; 3M, St. Paul, MN). Phosphate buffered saline (PBS) was prepared in deionized water using BupH™ Modified Dulbecco's PBS (Thermo Fisher Scientific, Waltham, MA, #28374) buffer packs with a final concentration of 8 mM sodium phosphate, 2 mM potassium phosphate, 0.14M sodium chloride and 10 mM potassium chloride at a pH of 7.4.

2.2.2. Microsphere size characterization

The H20/H50 glass microspheres were suspended in PBS at a final concentration of 1.0 mg/ml. 20 µl of the microsphere solution was mounted on the glass slide for imaging on an EVOS FL Auto Cell Imaging System (Thermo Scientific, Waltham, MA) using an Olympus UPlanApo 10X objective (0.4 NA). The diameter of microspheres was measured directly from transmitted light microscopy images. At least 5,000 microspheres for each H20 and H50 were measured by using Image J open-source software [66]. Image J particle analysis criteria applied to binary, thresholded images included a minimum circularity of 0.85 to eliminate non-solitary or broken microspheres from the size analysis. Histograms with a bin size 5 µm were prepared in Microsoft Excel.

2.2.3. H20 microspheres size sorting protocol

A set of wire mesh test sieves (VWR, Radnor, PA) were used to sort the H20 microspheres by size. The nominal mesh sizes used were 105 µm, 74 µm, 53 µm, and 25 µm. In the sieving process, 1 g of dry H20 microspheres were placed in the upper sieve and shaken overnight (>12 hrs) on a rotary shaker at 350 rpm, followed with manually shaking for 20 minutes. Each fractionated population was decanted from the respective sieve and stored at room temperature in clean glass vials.

2.2.4. Characterization of floatation properties

The floatation and buoyancy properties of the silica microspheres were characterized using time-lapse video and a UV/Vis spectrophotometer (Cary 60 UV/Vis; Agilent Technologies, Santa Clara, CA). 0.1g H20 or H50 particles were first placed into a 2 ml quartz cuvette. A time-lapse video was taken to visualize the microsphere migration in a 2 ml quartz cuvette. In the video, the cuvette was shaken three times manually, then allowed to stand still over 10 minutes. Still images were extracted from the video at 30 second intervals. Next, after another mixing the cuvette was placed into a UV/Vis spectrophotometer where the change in optical density (OD) was monitored at 450 nm wavelength violet visible light over 10 min. The separation time was calculated from the kinetic curves as the time point at which 90% of the total OD decline occurred ($0.9 \times (OD_{initial} - OD_{final})$). Various glycerol concentrations, from 0% – 50% in PBS, were used in this characterization to simulate the wide range of fluid densities and viscosities expected in biological fluids. Each of the size fractionated H20 microsphere populations were tested in PBS buffer and in 30% glycerol respectively. The viscosity of glycerol at 30% v/v (2.5

cP) is roughly equivalent to the viscosity or normal whole blood (3.2 cP) and plasma (2.0 cP) [67].

2.3. Results and discussions

2.3.1. Size distribution of H20 and H50 microspheres

We measured the diameter of H20 and H50 microspheres from microscopy images and generated histogram plots to examine the distribution of bead sizes present in each population. We found a wide range of particle sizes in the H20 population, from less than 10 µm in diameter to more than 80 µm in diameter, with a population mean of 27 ± 13 µm and a mode of 16 µm (Figure 5a). The H50 microspheres were slightly smaller with a mean diameter of 17 ± 7 µm and a mode of 12 µm (Figure 5b).

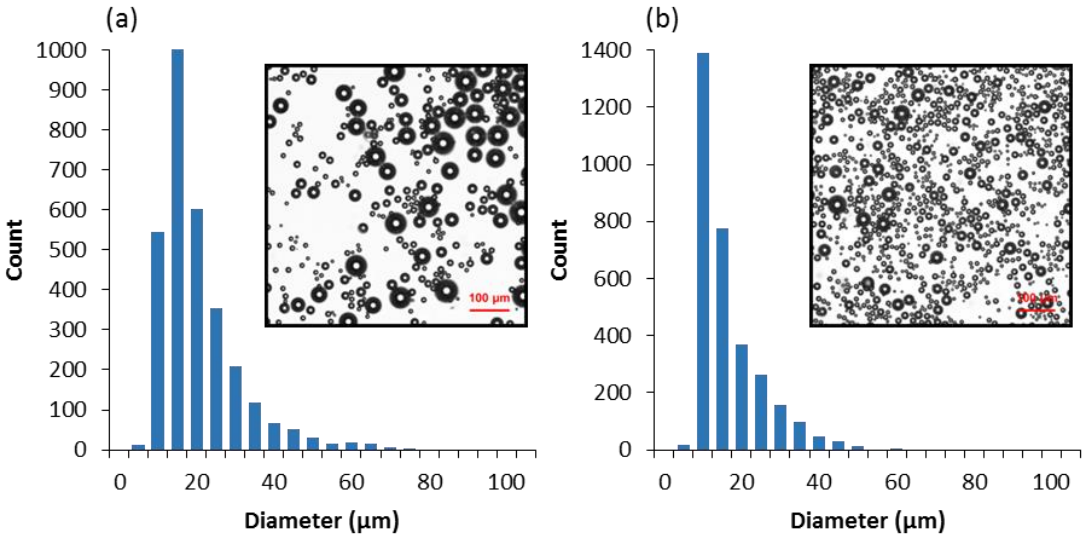

Figure 4. Histogram plot of the size distribution of (a) H20 and (b) H50 microspheres and a representative transmitted light microscopy image for each population. Scale bar is 100 µm.

2.3.2. Floatation kinetic of microspheres in different viscosity of solutions

The rate of H20 microsphere floatation was monitored by time-lapse video at 30 second intervals (Figure 6). In PBS buffer, the H20 microspheres began to migrate toward to the top of the buffer immediately when mixing was stopped. After about two minutes, nearly all of the microspheres were seen floating at the surface and the lower fluid fraction had nearly cleared.

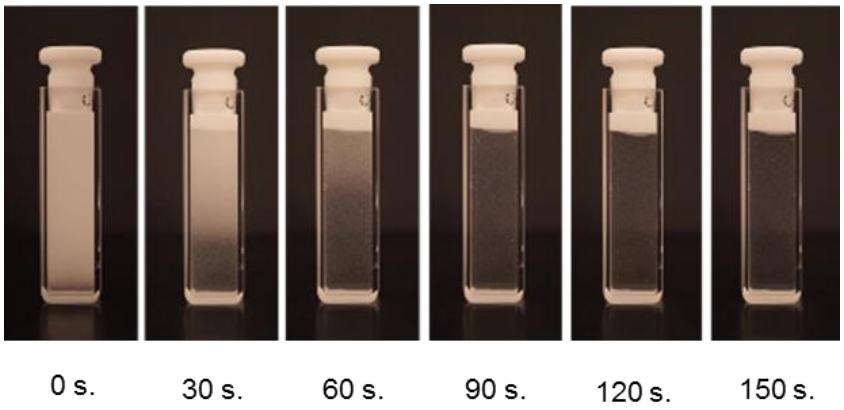

Figure 5. Photographs of H20 hollow silica microsphere floatation and separation at 30 sec intervals.

The optical density throughout the floatation-based separation process in PBS buffer, and solutions containing increasing amounts of glycerol for H20 and H50 microspheres are shown in Figure 7 a, and b, respectively. For both particle populations, the sharpest decline in OD occurred in the PBS buffer, which has the lowest viscosity. As glycerol content increased up to 50%, the rate of OD decline was progressively delayed for both the H20 and H50 microspheres.

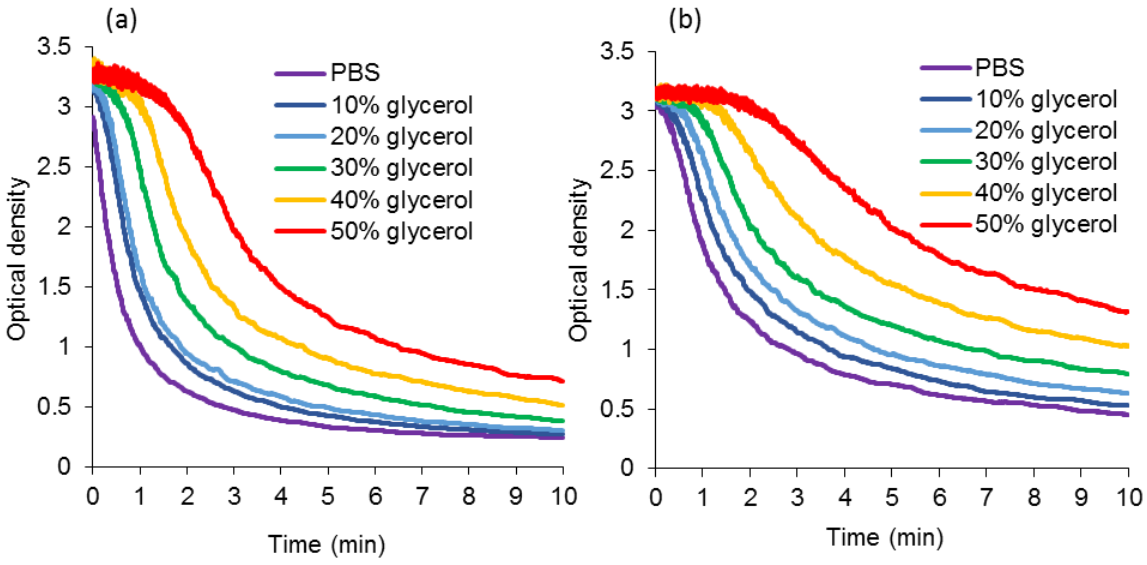

Figure 6. Kinetic traces from optical density measurements over 10 min for (a) H20 and (b) H50 microspheres in buffer solutions of increasing glycerol content (from 0 to 50%)

The microsphere separation time was calculated as the time point at which 90% of the total OD change had already occurred. For the H20 microspheres, the separation time was 2.7 minutes in PBS buffer and 6.7 minutes in the 50% glycerol/PBS solution. In the case of smaller H50 microspheres, the separation time was 4.7 minutes in PBS and 8.2 minutes in 50% glycerol. A complete list of separation times is provided in Table 4. Next, we plotted the H20 separation time versus literature values for the viscosity of glycerol (Figure 8) [68, 69]. As expected, based upon the forces acting on a submerged object, the separation time increased non-linearly with the fluid viscosity, which suggested that the viscosity was a key factor influencing separation time and efficiency for similarly sized particles. In addition, these results suggested that in biological fluids, such as blood whose viscosity is close to that of the 30% glycerol solution, separation times around 5 minutes could be achieved with the larger H20 microsphere population.

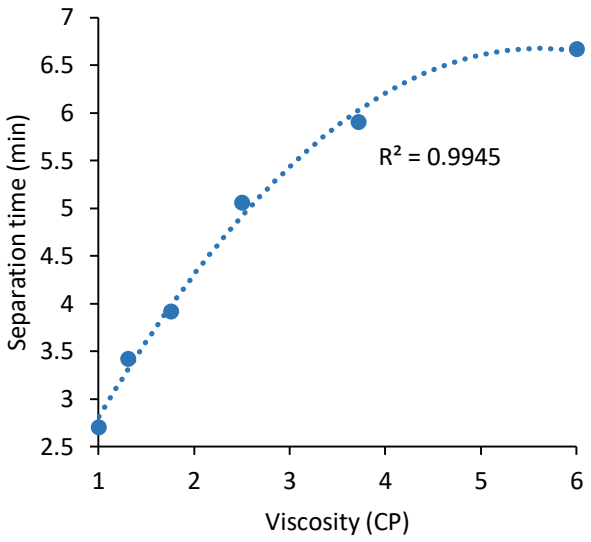

Figure 7. The separation time versus fluid viscosity for H20 microspheres.

2.3.3. Size-sorted microspheres

The bulk H20 microspheres were size fractionated in order to obtain a more homogeneous population which would be able to have more precise control of the buoyancy properties. By using wire mesh test sieves with mesh sizes of 105 µm, 74 µm, 53 µm, and 25 µm, respectively, the microspheres were separated into four relatively narrow size distributed microspheres populations with mean diameters ranked from smallest to largest of 21 ± 5 µm, 38 ± 7 µm, 62 ± 10 µm, and 81 ± 12 µm. Histogram plots and transmitted microscopy images of each population are shown in Figure 9. From the histogram, we also found that a few of the smaller particles could still be seen in the larger sieved populations. The small particles in large sized populations might due to imperfect sifting or attachment to larger microspheres.

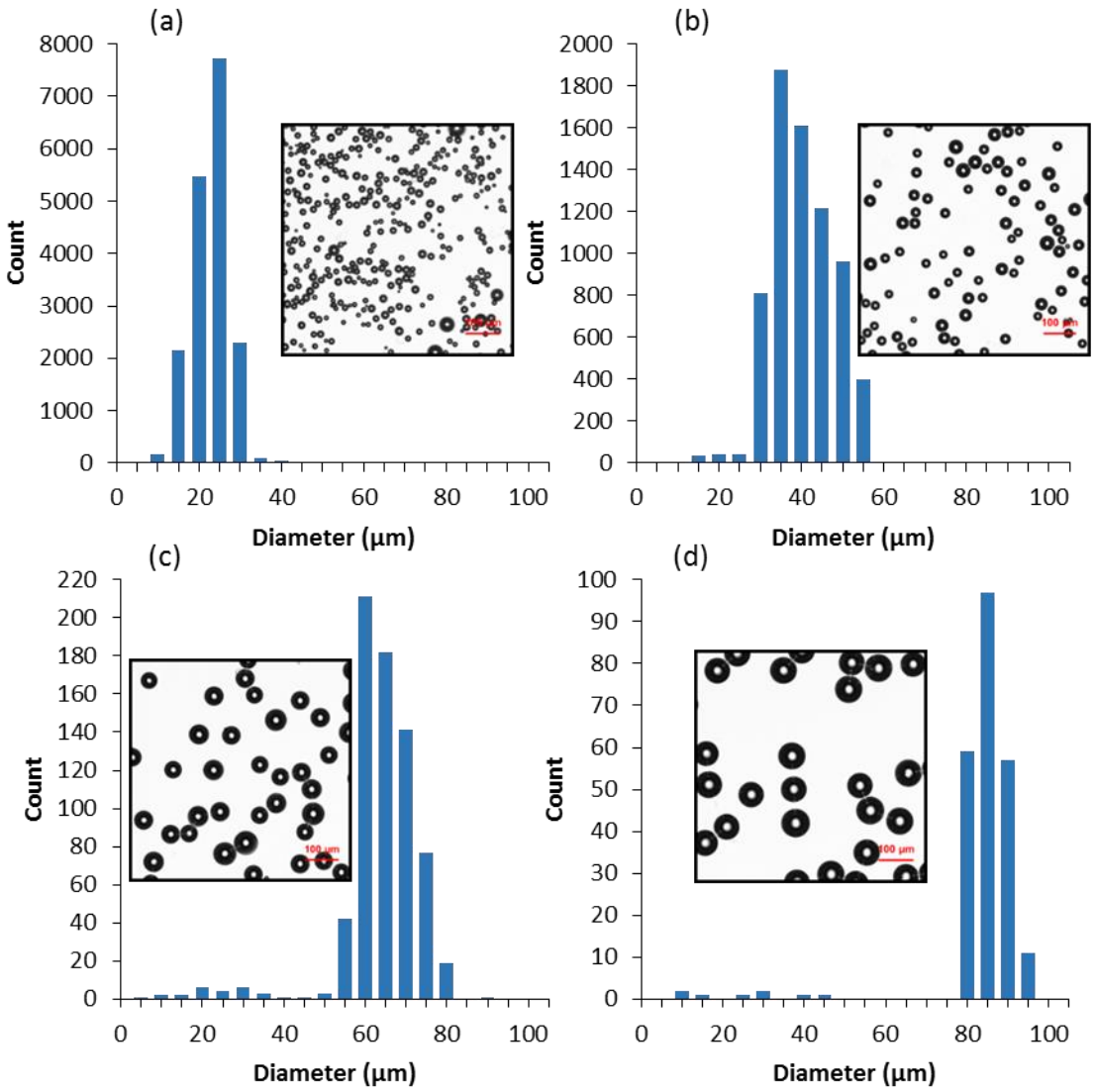

Figure 8. Histogram plots for the size fractionated H20 microsphere measured and phase-contrast microscopy images with mean of diameters of (a) 21 ± 5 µm, (b) 38 ± 7 µm, (c) 62 ± 10 µm, and (d) 81 ± 12 µm. Scale bare is 100 µm.

2.3.4. Floatation kinetics of different sized microspheres

Once we sorted H20 microspheres into narrow sized ranges, we monitored the rate of microsphere separation for each of these size-fractionated populations in PBS and 30% glycerol again, as previously done for the bulk H20 and H50 microspheres. The viscosity of glycerol at 30% v/v (2.5 cP) is roughly equivalent to the viscosity or normal whole blood

(3.2 cP) and plasma (2.0 cP) [67]; therefore, it was used as a surrogate for the viscosity expected in a biological fluid. As expected, the separation time was inversely proportional to microsphere size, which means the larger sized microspheres exhibited faster separation times over the smaller ones. In PBS buffer, the three largest bead populations all exhibited separation times under 30 seconds, while the separation time for the smallest (< 25 μm dia.) population was about 2.5 minutes (Figure 10a). In 30% glycerol, the separation time increased to ≤1 minute for the two largest populations and 2.2 minutes for the 25-53 μm diameter population, while the smallest set at < 25 μm did not achieve measurable separation over the 10 minutes measurement period (Figure 10b); however, they could ultimately float to the surface of the liquid within 30 minutes or more (data not shown). Compared to the H20 or H50 floatation kinetic results, the size-fractionated microspheres had steeper slopes (except the < 25 μm population in 30% glycerol), which indicated that the size-sorted microspheres had more uniformed buoyancy properties due to the homogenous size distributions; therefore, the buoyant force of each individual microspheres were within a narrow range of similarity.

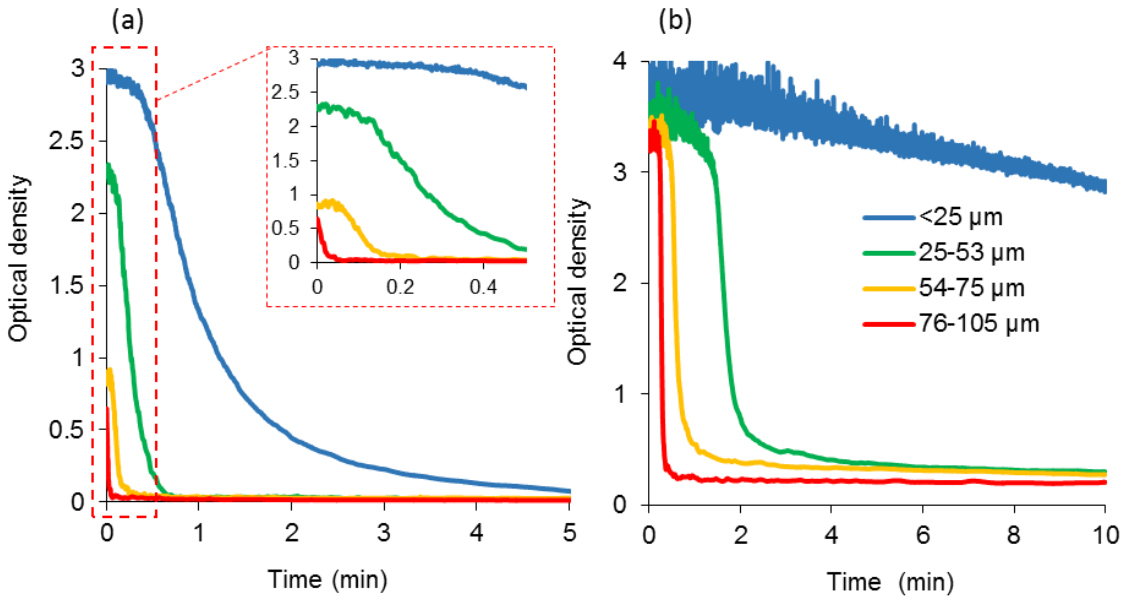

Figure 9. Kinetic traces from optical density measurements for size fractionated microspheres in (a) PBS buffer, and (b) 30% glycerol solution.

Table 5. Experimentally derived separation times in minutes for each of the hollow silica microsphere population, and the viscosity and density of different % of glycerol.

	0% glycerol	**10% glycerol**	**20% glycerol**	**30% glycerol**	**40% glycerol**	**50% glycerol**
H50 bulk	4.69	5.41	5.83	6.44	7.37	8.15
H20 bulk	2.71	3.42	3.92	5.06	5.91	6.67
<25 µm	2.46			--		
25-53 µm	0.47			2.23		
54-75 µm	0.17			0.92		
76-105 µm	0.05			0.33		
Viscosity* (cp)	1.005	1.31	1.76	2.50	3.72	6.00
Density† (g/ml)	1.0000	1.0207	1.0453	1.0706	1.0971	1.1239

* in water at 20°C; † in water at 25°C

The separation time for each size fractionalized populations were shown in Table 4. A plot of separation time in PBS buffer versus the mean diameter for each microsphere population in shown in Figure 11. The separation time closely followed a non-linear and inversely proportional relationship with the mean diameter of the microsphere.

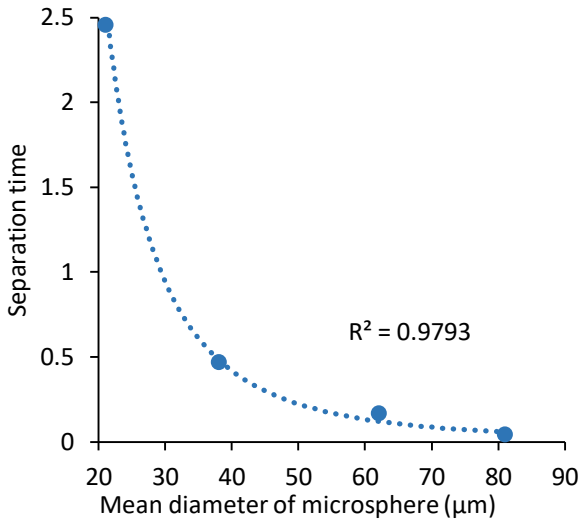

Figure 10. The separation time versus mean diameter of fractionated H20 microspheres.

2.4. Discussions

The flotation results that presented in this chapter can be better understood by revisiting a few principles of physics which describe the three forces acting on the particles (Figure 11). For a submerged object, the upward buoyant force is equal to the weight of the displaced fluid (Archimedes' principle) and can be calculated according to Equation 1 where ρ_f is the density of the fluid, V_f is the volume of the displaced fluid, and g is gravity (9.8 m/s^2). Submerged objects that rise in a fluid have a buoyant force that is greater than the sum of the two downward forces due to gravity and drag. The force of gravity is simply the weight of the object (mg), and can be written according to Equation 2 where ρ_o is the density of the object, V_o is the volume of the object, and g is gravity. The drag force, also known as the frictional force or Stokes' drag, on the object is given by Equation 3 where η is the fluid viscosity, r is the radius of a spherical object, and υ is the velocity [70]. When the net force is positive (Equation 5), the object will accelerate upwards until the object

reaches equilibrium where the net force is zero (the sum of forces $F_{net} = 0$) and the object is rising at a constant speed or it is floating on the surface of the fluid. Since the silica microspheres are hollow, the buoyant force is largely size-dependent with larger particles having less density and displacing a larger volume of fluid than smaller microspheres in a fluid with similar density/viscosity. As such, the magnitude of the positive net force is greater, despite an increase in both the gravity and drag force for larger particles than smaller particles. For example, the buoyant force acting upon the H20 microspheres with a mass of 2.06 ng is 1.01×10^{-7} N (calculated from Equation 1 and mean volume of the microspheres) while the H50 microspheres with a mass of 1.29 ng experiences a buoyant force of 2.52×10^{-8} N such that there is only 1.6-fold difference in mass, but 4-fold difference in the buoyant force. Thus, the larger and less dense hollow microspheres would be expected to have faster separation times in fluids with similar density/viscosity properties, as seen in the kinetic data above comparing separation times between the larger H20 (2.7 min in 0% glycerol) and smaller H50 microspheres (4.7 min in 0% glycerol). In addition, for similarly sized microspheres in high viscosity solutions, an increase in the drag force would be expected to reduce the net force and delay separation time, as seen when the H20 separation time was plotted against viscosity (Figure 7).

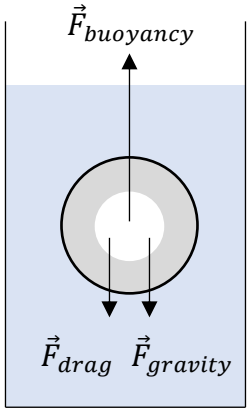

$$F_{buoyancy} = \rho_f V_f g \qquad \text{(Equation 2)}$$

$$F_{grav} = \rho_o V_o g = mg \qquad \text{(Equation 3)}$$

$$F_{drag} = 6\pi\eta r\upsilon \qquad \text{(Equation 4)}$$

$$F_{buiyancy} > F_{grav} + F_{drag} \qquad \text{(Equation 5)}$$

Figure 11. Force diagram and equations describing the three forces acting upon the hollow microspheres in a solution.

The floatation kinetic results also provide an experimental evidence for selecting proper-sized microspheres in different pathogen isolation applications. For example, the smallest sized microsphere population (< 25 μm diameter) would not be the best choice to be used for separating pathogens from whole blood sample, because the separation time is too long for them in the 30% glycerol test to be defined as rapid separation, and the 30% glycerol has a similar viscosity as the whole blood. On the other hand, the 76-105 μm has the shortest separation time, but at the same time, they have the least chance to interact with pathogens to compare with smaller sized particles.

2.5. Conclusions

The size-fractionated microspheres exhibited better uniformity of size and separation rate than the raw material, which helps us to have better control of the incubation time in surface functionalization and pathogen isolation. The study of microsphere

floatation kinetics also provides an evidence for microsphere selections in different applications.

III. SURFACE FUNCTIONALIZATION OF HOLLOW SILICA MICROSPHERES

3.1. Introduction

As described in previous chapter, the raw material 3M glass bubbles have already pre-treated with epoxy silane groups. The existing epoxide groups on the microsphere surface are able to react with various nucleophiles via a ring-opening reaction at different basic pH conditions [65]. Nucleophiles such as primary amines, hydroxyl groups, or sulfhydryl are able to attack the least saturated carbon of the epoxide ring via a Sn2 substitution reaction to form secondary amine, ether, and thioether bond under different pH conditions, respectively (Figure 12). Biomolecules, such as proteins and antibodies that were used in this study, contain many of these functional groups at the N-terminal or within amino acid side chains, such as lysine, to be able to conjugate onto the microspheres via this epoxide ring opening reaction.

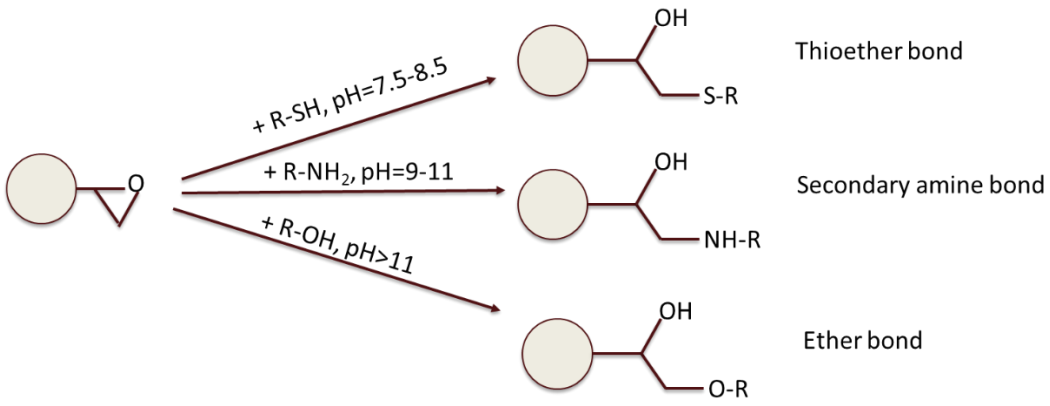

Figure 12. Epoxy silane surface chemistries available to conjugate biomolecule onto the microsphere surface.

Primary amine groups on protein one of the nucleophiles that enable to react with epoxide ring. The chemical reaction of primary amine and epoxide was shown in Figure 13, where the lone pair electrons on nitrogen attack the least hindered carbon of the epoxide ring to open the ring and form a new carbon-nitrogen bond via Sn2 substitution reaction. Once the carbon-oxygen bond is broken, the oxygen gained two electrons from the broken bond and become negative one charged, because the oxygen is more electronegative than the carbon. On the other side, since the nitrogen shared its lone pair electrons to the carbon and, four bonds were then on the nitrogen, and the nitrogen itself appeared to be positively one charged. The extra pair of lone pair electrons on the oxygen then attracted the hydrogen on the nitrogen to form a hydroxide group, thus, the primary amine group contained biomolecule covalently bound with the carbon chain by a secondary amine linkage.

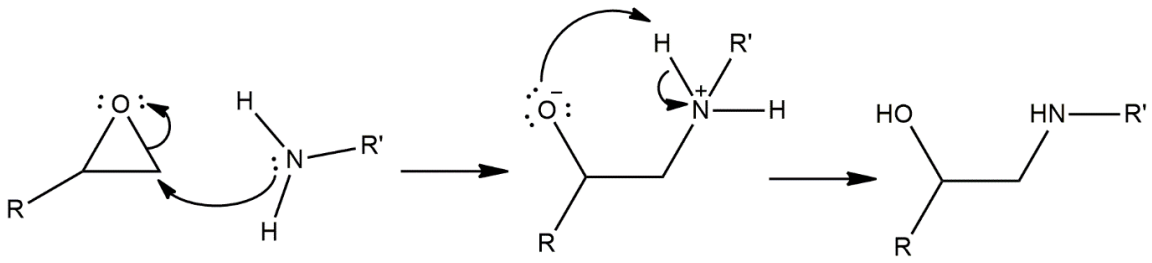

Figure 13. Chemical reactions of epoxied ring opening reaction for protein G immobilization.

3.2. Experimental methods

3.2.1. Materials and reagents

Buffers, protein G, and L-cysteine were all purchased from Thermo Fisher Scientific (Waltham, MA). 0.1 M sodium carbonate/bicarbonate buffer at various pH (range 9.1 – 10.5) was followed by published protocol [71] A goat-anti-mouse IgG conjugated to Alexa-Fluor®488 (GAM-AF488) (#A11001, Invitrogen, Carlsbad, CA) were used for quantitative imaging study.

3.2.2. Optimization of coupling buffer

Protein G (1.0 mg/ml) was incubated with 1 mg of the 25-53 µm fractionated microspheres in 100 µl (1.4×10^6 microspheres/ml) of PBS buffer (pH 7.4) and 0.1 M sodium carbonate/bicarbonate buffer at various pH (9.0, 9.5, 10, and 10.5), prepared according to published protocols [71], for 24 hours at 4°C with continuous end-over-end mixing. Microsphere concentrations (beads/ml and beads/mg) were obtained from hemocytometer counts of 1 mg of beads from 25 - 53 µm fraction resuspended in 100 µl 50% glycerol/PBS.

L-cysteine was added to a final concentration of 50 mM and incubated for another 24 hours to block any unreacted epoxy groups. After incubation, the microspheres were washed three times in PBS by tilting the microfuge tube ~45° allowing the particles to collect at the liquid surface, then removing the lower solute fraction and resuspending remaining particles in 500 µl PBS buffer. Functionalized particles were typically used immediately or stored at 4°C for up to one week. The presence of protein G on the microsphere surface was confirmed directly by scanning electron microscopy (SEM). The SEM images were taken at a high voltage electron beam of 5.0 kV and in 2000 times of magnification on a Helios NanoLab™ 400 DualBeam™ Scanning Electron Microscope (FEI, Hillsboro, OR).

The protein G surface functionalization for optimizing buffer pH conditions were also confirmed indirectly by fluorescence microscopy and quantitative image analysis of protein G bound to a secondary GAM-AF488 antibody. GAM-AF488 antibody was incubated with 1 mg protein G functionalized microspheres at a final concentration of 0.1

mg/ml in PBS, mixed for 2 hours at room temperature. After the incubation, excess unbounded antibodies were washed by 500 µl PBS buffer for tree times. 20 µl microspheres from each individual sample were then mounted onto glass slides for microscopy observations. Epi-fluorescent and transmitted light images were collected from at least 20 fields-of-view.

3.2.3. Determination of protein G binding capacity

Different amounts of protein G (0, 0.01, 0.05, 0.1, 0.5, and 1.0 mg/ml) was incubated with 1 mg of the 25-53 µm and 76-105 µm fractionated microspheres in 100 µl of sodium carbonate and sodium bicarbonate coupling buffer at a fixed pH = 9.5 for 24 hrours. L-cysteine was added to a final concentration of 50 mM and incubated for another 24 hours to block any unreacted epoxy groups. After the protein G coating and L-cysteine blocking processes, microspheres were washed by 500 µl PBS buffer for three times as described. GAM-AF488, at a final concentration of 0.1 mg/ml in PBS, was incubated with 1 mg protein G functionalized microspheres for 2 hours at room temperature with mixing. Epi-fluorescent and transmitted light images were collected from at least 20 fields-of-view and then exported to ImageJ for quantitative analysis. Analysis routines included automatic intensity thresholding, conversion to a binary mask, holes filled, and watershed applied to obtain region-of-interest (ROI) outlines for each particle with a minimum size of 500 pixels and circularity of 0.75. The intensities within the ROIs were measured on the original 8-bit grayscale image to obtain mean fluorescence intensity (MFI) per microsphere. Approximately 2,000 particles were measured at each protein G concentration run in

triplicate. Data was graphed in SigmaPlot and fit to an exponential rise-to-maximum curve with equation $f = y_0 + a(1 - e^{-bx})$.

3.3. Results

3.3.1. Optimization of coupling buffer for protein G immobilization

Our functionalization strategy relied upon a pH-dependent epoxide ring-opening reaction that covalently linked the epoxy silane treated microspheres to biomolecular functional groups (-NH_2, -SH, and -OH) in protein G. Protein G is an immunoglobulin (IgG)-binding protein expressed in group *C* and *G Streptococcal* bacteria [72]. Protein G has a strong affinity to IgGs from different species, especially human and mouse. In addition, protein G contains multiple Fc-binding domains, which will specifically bind to the Fc portion of the immunoglobulin G, and the antigen recognizing domains of antibody were freely available to bind pathogen targets. The overall functionalization schematic showed in Figure 14, which indicates the two steps functionalization by first covalently bind the ring-opened epoxide groups and the primary amine groups on the protein G at pH over 9, and then immobilizing target-specific IgG antibodies on the protein G.

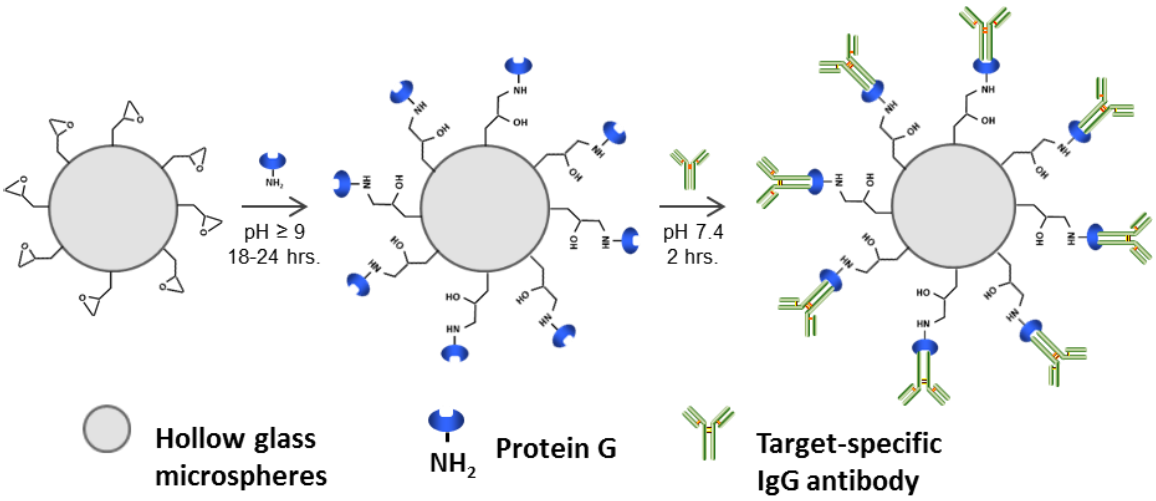

Figure 14. Schematic of fully functionalized microspheres with protein G followed by a target-specific IgG antibody.

The SEM images were taken for raw and protein G coated 25-53 µm microspheres respectively. SEM imaging of the unfunctionalized microspheres appeared to have a relatively smooth surface with some minor defects present (Figure 15 a). After the immobilization of protein G, a number of protein "patchy islands" were visible on the surface (Figure 15 b), which suggested the successful attachment of protein G. EDAX element analysis for both blank microsphere and microsphere coated with protein G were shown in the Appendix section Figure S1. The element analysis indicated that only O and Si were found on the blank microsphere, while the protein G coated microsphere contained C, O, Na, and Si, due to the of protein G attachment and buffer salt.

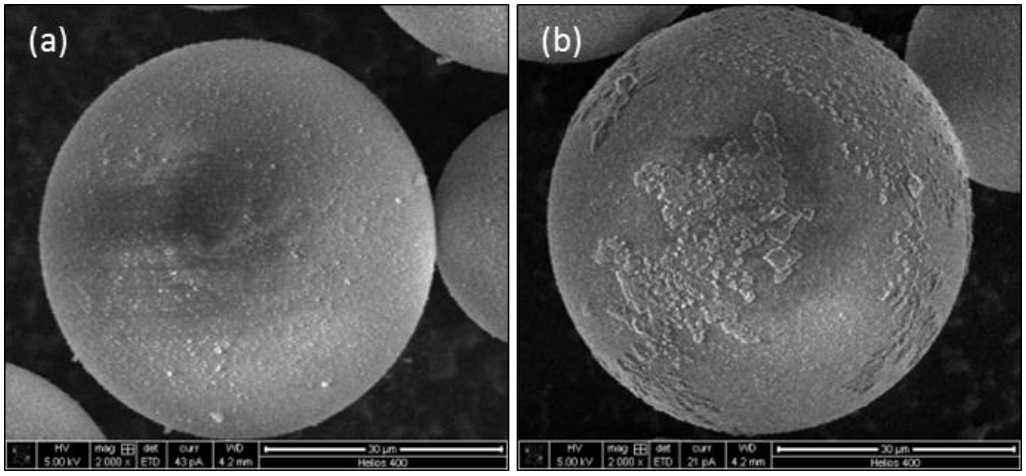

Figure 15. SEM images of 25-53 µm microspheres before protein G coating (a) and after coated with protein G (b).

Optimizations of protein G immobilization were further evaluated by using a secondary GAM-AF488 antibody under various buffer conditions (PBS buffer pH = 7.4, Carbonate/bicarbonate buffer pH = 9.0, 9.5, 10.0, and 10.5), and epi-fluorescent imaging. From the epi-fluorescent images shown in Figure 16, we could see that conjugation occurred in both PBS and coupling buffer at all pH conditions tested. Visual assessment of the images from Figure 15 established that the carbonate/bicarbonate buffer at pH 9.0 provided the most intense and uniform coating of protein G on the microspheres. All subsequent experiments utilized these optimized conditions for protein G functionalization.

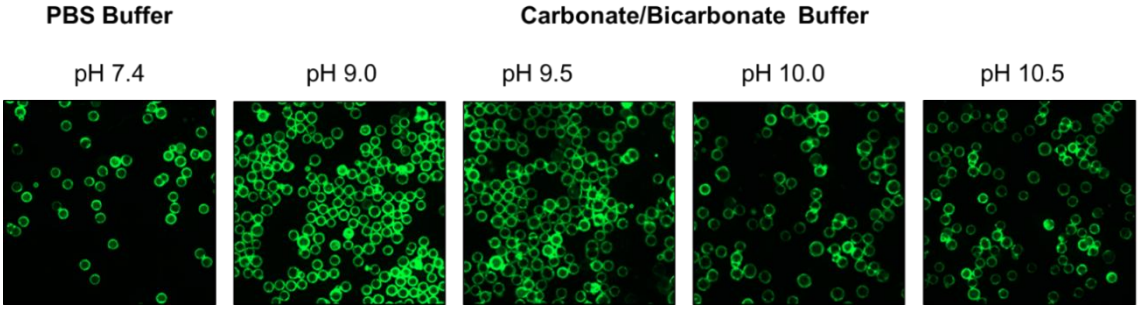

Figure 16. Epi-fluorescent images for different buffer and pH conditions (PBS buffer, pH 7.4; carbonate/bicarbonate buffer pH 9.0 – 10.5).

3.3.2. Examination of microsphere protein G binding capacity

After the best buffer condition of surface immobilization was found, we further examined the binding capacity of protein G on the microsphere surface. Here, different amounts of protein G was coated onto 1 mg of the 25-53 µm and 76-105 µm fractionated microspheres using optimized conditions established above. Saturating concentrations of GAM-AF488 antibody enabled visual confirmation of protein G attachment versus negative controls with no protein G. The epi-fluorescent and transmitted light images for 25-53 µm and 76-105 µm microspheres are shown in Figure 16a and Figure 17a, respectively. The fluorescent intensity increased progressively with the protein G concentration in both of the 25-53 µm and 76-105 µm microspheres. In addition, the fluorescent image of negative control samples had nearly no fluorescent signal visible, which suggests that the L-cysteine sufficiently blocked the microsphere from nonspecific binding (Figure 17 and 18).The fluorescence intensity of each microsphere sample was then quantitatively analyzed by ImageJ. The exponential curve fit for 25-53 µm and 76-105 µm microspheres are shown in Figure 17b and Figure 18b, respectively. The protein G binding capacity of microspheres was determined by calculating the protein G concentration at the 95% maximum saturation. The 95% of fluorescent intensity occurred at 0.31 mg/ml protein G concentration for 25-53 µm microspheres, and 0.50 mg/ml for the 76-105 µm microspheres. Hence, since 1 mg microspheres were incubated with 100 µl protein G, the binding capacity was 31 µg/mg and 50 µg protein G/mg microsphere for 25-53 µm microsphere and 76-105 µm microspheres, respectively.

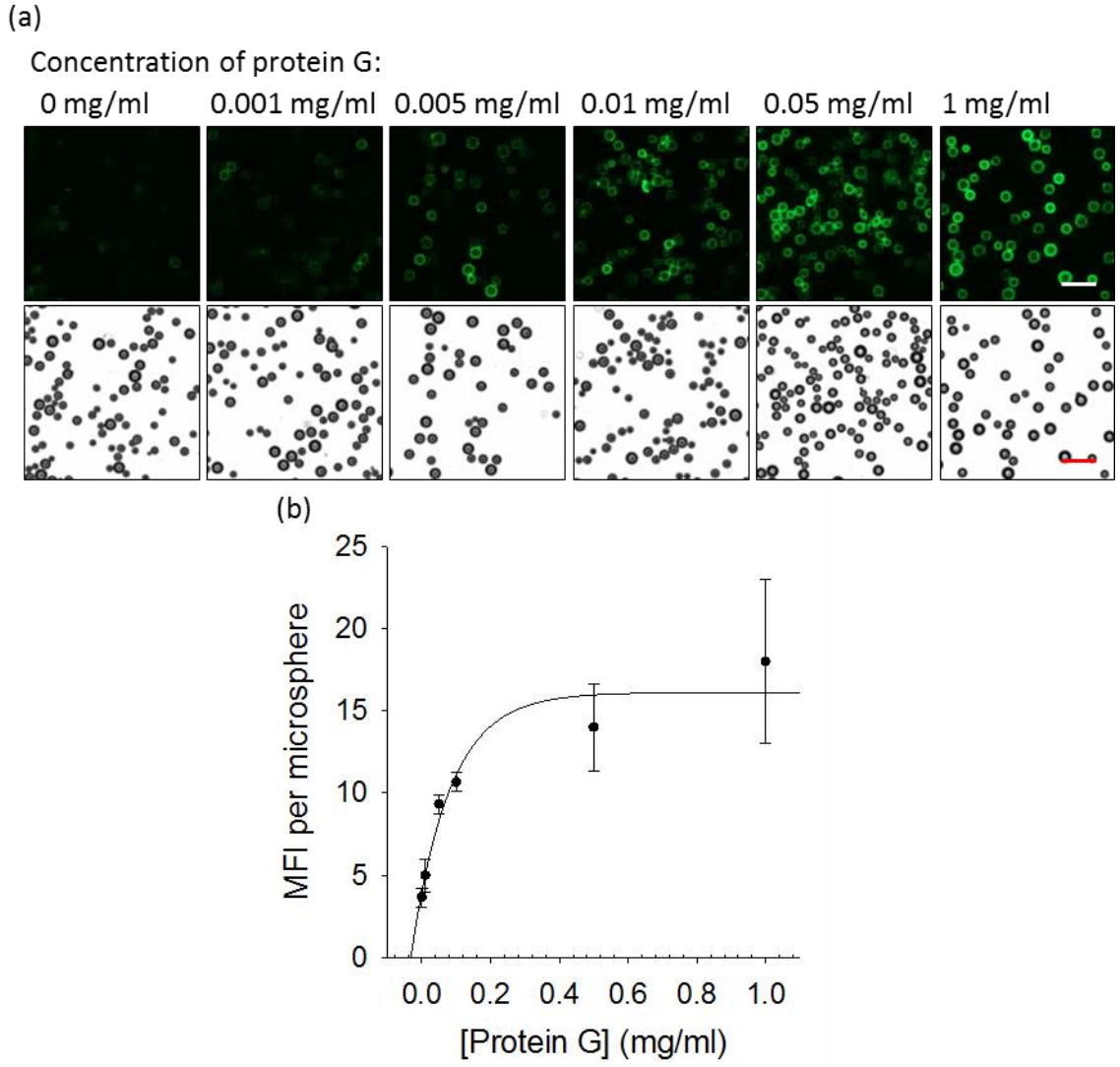

Figure 17. (a) Epi-fluorescent and bright-field images of fully functionalized 25-53 µm microspheres at increasing concentrations of protein G (left to right, 0 mg/ml control, 0.01 mg/ml, 0.05 mg/ml, 0.1 mg/ml, 0.5 mg/ml and 1.0 mg/ml, respectively). Scale bar is 100 µm. (b) Quantitative mean fluorescence intensity (MFI) data fit to an exponential curve for 25-53 µm microspheres.

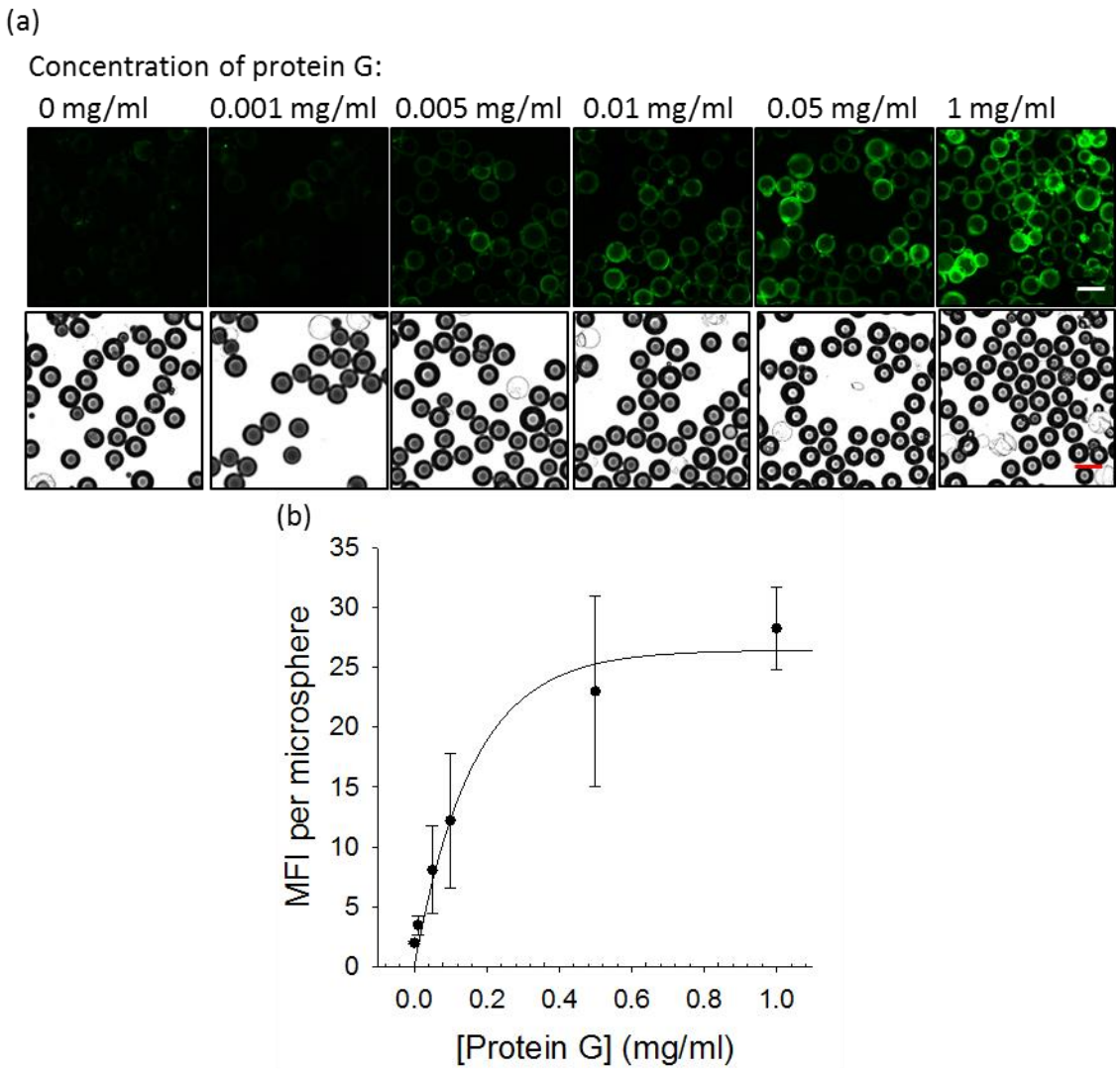

Figure 18. Epi-fluorescent and bright-field images of fully functionalized 76-105 µm microspheres at increasing concentrations of protein G (a-e, 0 mg/ml control, 0.01 mg/ml, 0.05 mg/ml, 0.1 mg/ml, 0.5 mg/ml and 1.0 mg/ml, respectively). Scale bar is 100 µm.

3.4. Discussions

In this chapter, we established the method of microsphere surface functionalization with protein G via epoxide ring opening reaction, followed by a protein G-mediated binding of IgG. SEM confirmed the presence of protein G on the microsphere surface (Figure 14), presumably via the epoxide ring opening reaction with primary amine or other

functional groups present. Uncoated microspheres exhibited a relatively smooth surface with some small dust or particulates. However, the SEM image of protein G coated microsphere appeared to have an irregular and uneven distribution of protein distributions on the surface of the microsphere. The “patchy island” formation of the protein G on the microsphere might because the denaturation of protein caused by the drying protocol for SEM imaging operational needs. However, the protein G was immobilized more evenly distributed on the microsphere when they were hydrated, because from the epi-fluorescent images in Figure 16 we could found the microspheres were coated with fluorescently labeled antibodies uniformly.

To compare across all of the results, the fluorescent signals had the highest intensity and uniformity at pH = 9 buffer condition was due to several reasons. First, at pH = 9, primary amine has better activity to react with epoxide. Second, according to the amino acid sequence of protein G reported from National Center for Biotechnology Information (NCBI, Accession # AAB06623), the primary amine groups (42 lysine) are more abundant than the sulfhydryl groups (2 cysteine). Third, although the primary amine group has a preferred pH range from 9 to 11, the high pH of buffer also could influence the protein activities, thus the GAM-AF488 antibodies were less efficiently bind with protein G in high pH conditions (9.5, 10,and 10.5) than in the pH = 9 buffer.

The binding capacity of 25-53 µm and 76-105 µm microspheres were 31 and 50 µg protein per mg of microspheres respectively. Commercially available magnetic nanoparticles have a binding capacity range from 20 to 400 µg protein per mg particle, the binding capacity of the microspheres fall into the range of those existing techniques. Typically in nanoparticles, such as magnetic beads, the protein binding capacity of smaller

particles are greater than the large sized ones due to the curvature effect, which the small beads have larger curvature to avoid hindrance between immobilized proteins [73]. However, this curvature effect was not applied in the microspheres because the size of our microspheres are ten to a hundred fold larger than nanoparticles, the surface of the microsphere is more of considered as a flat surface in biomolecular level, thus the one with larger area of surface resulted in having greater protein binding capacity. The surface area calculations of both the hollow centered microspheres and solid centered nanoparticles were summarized in Table 6. According to the calculation, smaller sized particles have greater surface area to volume ratio for both of nanoparticles and microspheres. However, the total surface area per 1 mg of the larger hollow microspheres was greater than the smaller sized ones, which was opposite to the solid nanoparticles, where the smaller particles have greater total surface area per mass. Instead of having constant density for both large and small particles like solid nanoparticles, the larger microspheres have much smaller density than the small-sized microspheres, which allowed large microspheres have only 1.8-fold less of particles per 1 mg than smaller particles, while the surface area per larger microsphere was 4.5-fold greater than smaller microsphere. Thus, the larger and less dense hollow microspheres have greater total surface area per mass. In contrast, although the 200 nm solid nanoparticles have 4-fold greater surface area than 100 nm particles, the number of the 200 nm particle was 8-fold less than smaller ones, due to the same density. Therefore, the smaller solid nanoparticles have greater total surface area per mass. The greater total surface area of the larger microspheres also explained why the binding capacity of larger microspheres were greater than the smaller particles.

Table 6. Calculation of surface area properties of hollow microsphere and solid nanoparticles

Material type	Diameter (cm)	Surface area per particle (cm^2)	Volume per particle (cm^3)	Mass per particle (g)	Number of particle per 1 mg*	Density (g/ml)**	Surface area to volume ratio	Total surface area per 1 mg particles (cm^2)
Microsphere	3.8E-03	4.5E-05	2.9E-08	7.1E-09	1.4E+05	0.25	1.6E+03	6.4
	8.1E-03	2.1E-04	2.8E-07	1.3E-08	7.7E+04	0.05	7.4E+02	15.9
Nanoparticle	1.0E-05	3.1E-10	5.2E-16	4.1E-15	2.4E+11	7.87	6.0E+05	76.2
	2.0E-05	1.3E-09	4.2E-15	3.3E-14	3.0E+10		3.0E+05	38.1

* The number of microsphere per 1 mg was experimentally counted by hemocytometer,
** The density of nanoparticle was the density of iron

3.5. Conclusions and future directions

In this chapter, we demonstrated successful microsphere functionalization with protein G and subsequent protein-G-mediated IgG binding capability. Additional work is needed to examine the stability of functionalized microspheres in terms of how long protein G coated microspheres could be stored in solution, or freeze-dried and maintain the same IgG binding functionality. Future studies could also utilize a direct method for estimating the binding capacity. For the binding capacity test, we used an indirect measurement of protein G attachment through a fluorescently labeled secondary antibody, but this indirect characterization method may not have the most accurate result. However, directly bind with fluorescently labeled protein G is not a viable strategy either because fluorophore conjugation would use the same functional groups that are needed for epoxide ring opening reaction with microspheres. Besides, instead of using epoxide reaction to bind protein G then immobilize antibodies, some other surface functionalization methods may also be examined, such as poly ethylene glycol (PEG) surface functionalization, and streptavidin-biotin linkage approach.

IV. CRYPTOSPORIDIUM CAPTURE AND DETECTION IN A PAPER-BASED MICROFLUIDIC TEST

4.1. Introduction

In Chapter 3 the surface functionalization and binding capacity of the microspheres were characterized. The protein G dose-dependent target-specific antibody immobilization allowed us to have a control of the amount of antibody on beads. Besides, the use of L-cysteine appeared to have an effective blocking effect to prevent nonspecific binding of antibodies or non-target analytes. In order to apply this separation technique into pathogen bioseparation, the experiment for utilizing functionalized microspheres isolate the pathogens from biological fluid is critical. In this chapter we will detail the results that we applied the anti-*Cryptosporidium* functionalized microspheres in the use of *Cryptosporidium* oocysts isolation in both PBS buffer and real stool samples. In addition, we designed a paper-based diagnostic device to integrate with the microsphere separation technique to further diagnose and quantify the isolated crypto oocysts.

4.1.1. Importance of *Cryptosporidium* in world health

Cryptosporidium is a waterborne parasite that causes gastrointestinal illness with chronic and/or persistent diarrhea in humans. *Cryptosporidium* is one of the most common causes of diarrheal illness, especially in some of under-developed and developing countries. Therefore, the development of rapid diagnostic tests for *Cryptosporidium* has attracted great attention in an effort to address this global health issue. However, laboratory instrumentations are still required for isolating *Cryptosporidium* from stools or water samples, as well as the well-trained technicians to operate, which may not be economically

feasible for the under-developed counties. Furthermore, existing parasitic eggs and oocysts separation methods, such as fecal floatation, still lack adequate recovery rate, and centrifugation is required [62-64]. In order to overcome the detection limitation of current methods, Iqbal et al. currently reported to detect *Cryptosporidium* via aptamer [74], but the instrumentation and cost issue still were still existing. Thus, in order to improve the detection limits, isolating and concentrating *Cryptosporidium* oocysts using the proposed "molecular buoy" concept prior to downstream analysis or counting could be an efficient way to enhance existing detection limits. Moreover, the microsphere density-based bioseparation technique would be particularly impactful in developing countries due to the low-cost of materials, independence from external instrumentation, and rapid separation times.

4.1.2. Paper-based microfluidics

In the last 50 years, the health technology has dramatically improved more than in the previous hundreds of years [75]. The development of POC is also greatly advanced to meet the diagnosing requirements in limited resource health settings in recent several decades. The World Health Organization (WHO) defined the POC diagnostic devices as "Affordable, Sensitive, Specific, User-friendly, Rapid/robust, Equipment free and Deliverable to end-users" (ASSURED) instruments [76]. Due to the features of low cost, easy to fabricate, and the biodegradable ability, paper become a good candidate for many POC diagnostic applications [77-80]. In 1956, a paper-based lateral flow immunoassay (LFIA) was first reported by Singer and Plotz [81]. Since then, the LFIA diagnostic device has continued to evolve and develop to become one of the most successful POC platforms

in the current POC market [82]. Commercially, the Alere Inc. is the POC market leader which occupied approximately 35% of the market share [82]. The commercially available LFIA devices have a variety of diseases detection categories include infectious diseases, cancer, cardiac diseases, and the most famous pregnancy tests [83]. The LFIA uses paper, nitrocellulose, or polymers that transport biofluid sample via only capillary action to separate, capture, and finally detect the target analytes in the sample, thus external instrumentations are eliminated. Typically, the LFIA paper chips were pre-loaded with target-specific antibodies at detection line and non-target-specific antibodies at control line. When the labelled antibody bound target analytes migrate to the detection line, a labeled antibody-antigen-antibody sandwich structure will form, while the access labelled antibody will bind with the control antibody with or without the target antigen to demonstrate the assay is working [84]. The result interpretation of the LFIA was usually determined by only visual optimization to evaluate the presence or absence of detection line and control line [85]. Therefore, the LFIA achieved the goal of cost elimination not only by using low-cost materials, such as paper and polymers, but also free of using external instrumentations for signal analysis.

In 2008, an evolution of LFIA platform called 2-dimentional microfluidic paper analytical devices (μPADs) was first established by Whitesides' group at Harvard University [86, 87]. In addition to the traditional LFIA devices, the 2-D μPADs use hydrophobic materials patterning out microfluidic channels, therefore, samples can be not only absorbed and transferred toward to detection area, but also can be direct by microfluidic channels for further separation or more complex treatments to make the Lab-on-a-paper concept feasible [86, 88, 89]. More recently, the single layered 2-D μPADs was

further developed by Whitesides' group by stacking multiple layers of μPADs and form a 3-D μPADs structure [89, 90]. Instead of migrating through the microfluidic channel horizontally on 2-D μPADs, samples can be directed in both horizontal and vertical ways in a 3-D μPADs. By controlling the design of the microfluidic channel, porous size, and types of materials of each paper layers, different biomolecules can be separated and directed, thus, enhance the separation effect and the limit of detection [90].

In this dissertation work, our goal is to develop an "ASSURED" 3-D paper diagnostic that integrated with the microsphere separation technique to achieve the truly external instrumentation free application from the sample preparation to the final diagnosis for detection of food or water pollution by pathogens, among others.

4.1.3. Integration of molecular buoy and paper-based microfluidic techniques

An overall schematic of the microsphere separation and paper detection are shown in Figure 19. Here, microspheres functionalized with anti-*Crypto* monoclonal antibody are mixed with an unknown stool sample. The antibody captures the *Cryptosporidium* oocysts that are present in the sample and carry them to the liquid-air surface due to the low-density of the microspheres. At this point, buffers are added above the maximum volume of the microfuge tube forming a positive meniscus. Since the microspheres float, when the meniscus is formed, beads with/without bound pathogens will be concentrated at the very top of the meniscus. By capillary action, the microspheres and any bound pathogens are collected directly onto the paper-based diagnostic device by simply touch the sampling area of the device on the meniscus. Next, a series of immunoassay reagents, buffer, and

colorimetric enzyme substrates generate direct positive/negative test results. A positive test should yield a faint/strong blue color while a negative test should yield no color change.

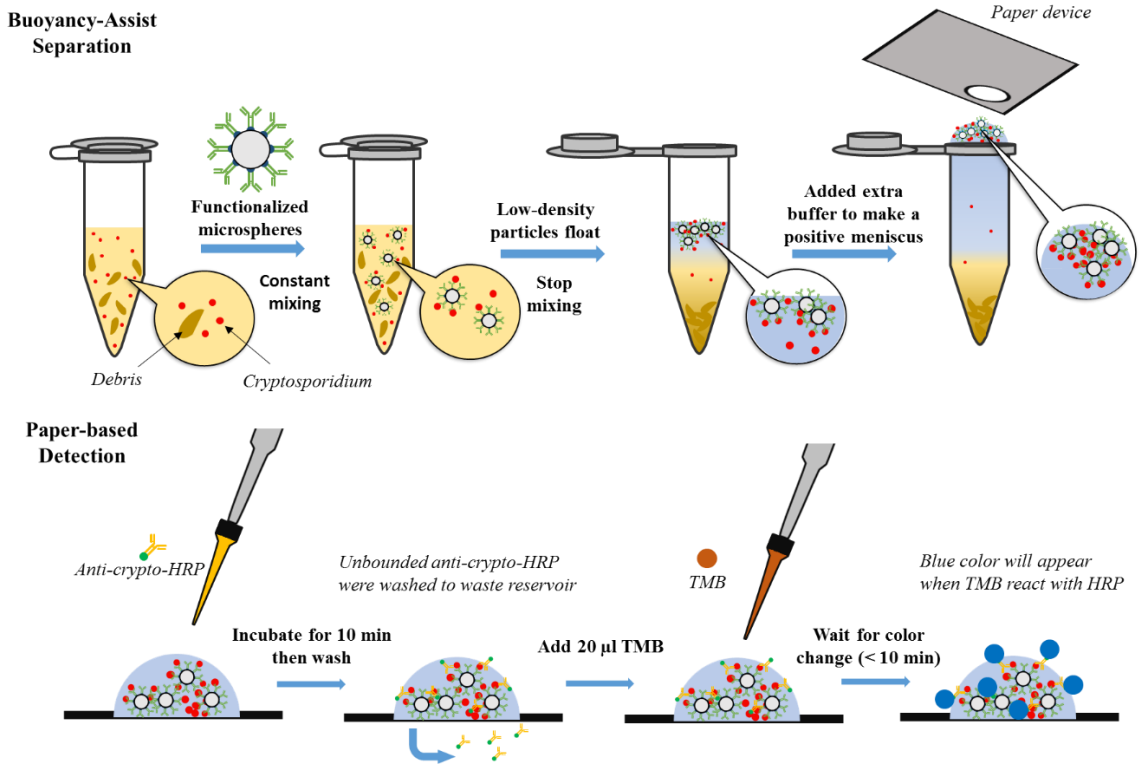

Figure 19. Schematic of buoyance assisted microsphere separation method integrate with paper-based detection.

4.2. Experimental methods

4.2.1. Materials and reagents

Sodium dodecyl sulfate (SDS) and 3,3',5,5'-Tetramethylbenzidine (TMB) were purchased from BIO-RAD (Hercules, CA). TWEEN® 20 was bought from Sigma-Aldrich (St. Louis, MO). Protein G, and L-cysteine were both purchased from Thermo Fisher Scientific (Waltham, MA). *C. parvum* oocysts (Iowa isolate, #P102C) and negative control stool were purchased from Waterborne Inc. (New Orleans, LA). Antibodies included an

unconjugated anti-*C. parvum* monoclonal mouse IgG3 (clone BEL 0126, #64526, Novus Biologicals, Littleton, CO), an anti-*C. parvum* directly conjugated to Alexa-Fluor®488 (clone BEL 0126, #2402-3007AF488, Bio-Rad AbD Serotec, Raleigh), and anti-*C. parvum* polyclonal goat IgG conjugate with horseradish peroxidase (HRP) (PA1-73185, Thermo Scientific Pierce, Waltham, MA).

The paper that was used for paper-devices is Chromatography paper (Whatman™, #3001-861) purchased from GE Healthcare Life Sciences (Chicago, IL). Absorbing pad (Cellulose fiber sample pads #102107) was purchased from Millipore (Billerica, MA). The design of the paper microfluidic channels was made by Adobe Illustrator® CS 6.0 software (Adobe Systems, San Jose, CA). Wax printing was done by Xerox® Phaser 8640 wax printer (Xerox Corporation, Norwalk, CT). SelfSeal™ transparent laminates were purchased from GBC (San Diego, CA). Printed paper devices and transparent laminates were cut by Universal® Laser Systems VLS4.60 laser cutter (Universal Laser Systems, Inc., Scottsdale, AZ).

4.2.2. Capture efficiency of molecular buoys using *C. parvum* oocysts

4.2.2.1. *Cryptosporidium* capture and imaging via fluorescence microscopy

First, 25-53 µm microspheres were coated with protein G. Protein G-coated microspheres were prepared as described in the previous chapter, by using 0.1 mg/ml protein G in 100 µl sodium carbonate/bicarbonate buffer at pH = 9.1, followed by blocking with L-cysteine at a final concentration of 50mM. The control microspheres did not contain protein G, but blocked with L-cysteine.

For qualitative imaging studies, 10^5 of the *Cryptosporidium* oocysts were pre-labeled with 0.01 mg/ml anti-Crypto/Alexa-Fluor®488 for 2 hours, washed 2 times by centrifugation at 5,000 rpm, supernatant removed then added them to protein G-functionalized microspheres for capture of the antibody and oocyst complex. After 2 hour of incubation, microspheres were isolated and mounted onto glass slides and observed via epi-fluorescent microscope. An Olympus FV100 Scanning Confocal Microscope with a 60X PlanApoN oil-immersion objective (1.4 NA) was used for confocal imaging (Olympus Corporation, Tokyo, Japan). In the confocal imaging experiment, 10^5 of the *Cryptosporidium* oocysts were added after the 2 hours antibody incubation, the excess antibody from the functionalized microspheres. Therefore, oocysts were captured by anti-Crypto immobilized on the microspheres and fluorescently immune-labeled by free antibodies at the same time.

4.2.2.1. Quantitative analysis and efficiency

For capture studies, both of the protein G-coated and control microspheres were incubated with unconjugated anti-*Cryptosporidium* IgG (0.01 mg/ml in PBS) for 2 hours at room temperature and washed three times by 500 µl PBS buffer. Microspheres were then mixed with either buffer or stool samples spiked with 10^2, 10^3, 10^4, and 10^5 *Cryptosporidium* oocysts in 100 µl for 2 hours. Following a 2 min floatation-based separation step, the lower fraction contained unbound oocysts was transferred to a new microfuge tube. The unbound oocysts that were remaining in the lower fraction were counted using a hemocytometer. At the lower oocyst concentrations, the lower fractions of the samples were centrifuged at 5,000 rpm for 5 minutes for counting purposes. After 5

minutes centrifugation, supernatant was removed, the concentrated oocysts pellets were resuspended in 20 µl PBS buffer and then counted by hemocytometer. The difference between the total number of oocysts input into each sample and the number recovered in the unbound fraction was used to calculate the percent oocysts bound by the functionalized microspheres. Three independent replicates at each oocyst concentration were run in PBS buffer and two in stool. A one-tailed t-test was performed in SigmaPlot to determine significant differences between positive/negative control samples and between PBS/stool samples containing the same number of oocysts ($p < 0.05$).

4.2.3. Design and assembly of the paper-based devices

The design of the paper microfluidic channel was done by Adobe Illustrator CS 6.0. The designed device were printed by Xerox® Phaser 8640 wax printer. The printed papers were heated by oven at 80°C for 1 minute to make the printed wax melt and soak into the paper fabric. After cooling down to the room temperature, paper devices were cut by Universal® Laser Systems VLS4.60 laser cutter. After cutting, devices were stocked in desiccators at room temperature to prevent the devices absorbing water from the air. A transparent single-side adhesive laminate was also designed by Adobe Illustrator CS 6.0 software, and then cut by Universal® Laser Systems.

The design of the paper device was shown in Figure 20, it has four types of square pieces with the same width of 30 mm, the area with colors were printed with wax, and the white part was the microfluidic channel, where the sample liquids are directed. The square area in the center of the paper is the sampling piece, which was designed for loading the microspheres onto the white circular sampling area. The sampling area was designed as a

7 mm diameter circle, which was the same size of the opening of a conventional 500 µl microfuge tube for the convenience of microsphere transferring. The red piece at the left side was a liquid directing layer, it was folded right underneath the sampling pad. The opening area for the red pad was a shape of arrow, the arrow had a round bottom, which is the same size with the sampling circle. In addition, the round bottom of the arrow would be completely overlap underneath the sampling area when it was folded. The arrow shape was designed to direct washing buffers to the far side of the sampling area to limit the background interference of the colorimetric detections. The length of the triangle side was 25 mm, which was designed as the maximum size of the shape to have the maximum of the area to reserve the washing buffers. Two reservoir pads were designed as blue color located at the top and bottom side of the sampling pad. Those reservoir pads had triangle shaped opening areas as the same size of head of the arrow, those pads would be right underneath the red arrow pad after folding. The bottom of the arrow was above the blue wax part of the reservoir pads, which provide a hydrophobic bottom under the arrow tail to direct washing liquids move toward to the reservoir. The yellow pad was fully covered by wax print, which was functioned as a hydrophobic bottom of the paper device.

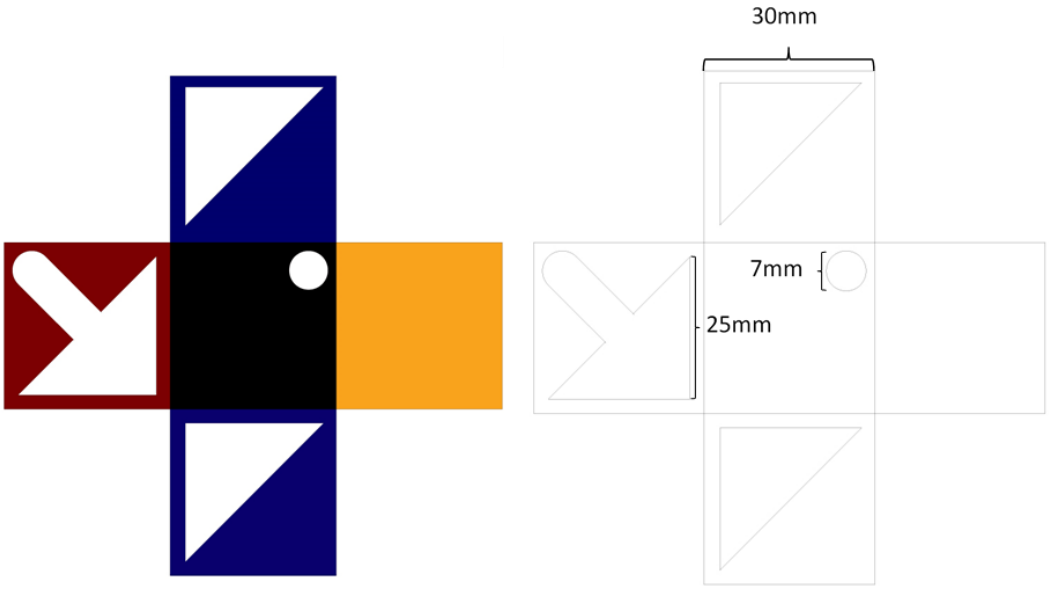

Figure 20. Design of foldable paper diagnostic device with its parameters.

The cut paper devices were assembled by simply folding the paper step by step when they were going be used. The folding follows the order of red, blue, blue, insert absorbing pad, and yellow bottom (RBBAY), showed in Figure 21. Folded devices were aligned with transparent single-sided laminate to enhance the contact of each paper layer. The laminate designation and a picture of laminated paper device were displayed in Figure 22. The width and length of the laminate were 40 mm and 70 mm respectively, which had a 5 mm margin for each sides to stick and laminate the folded paper device.

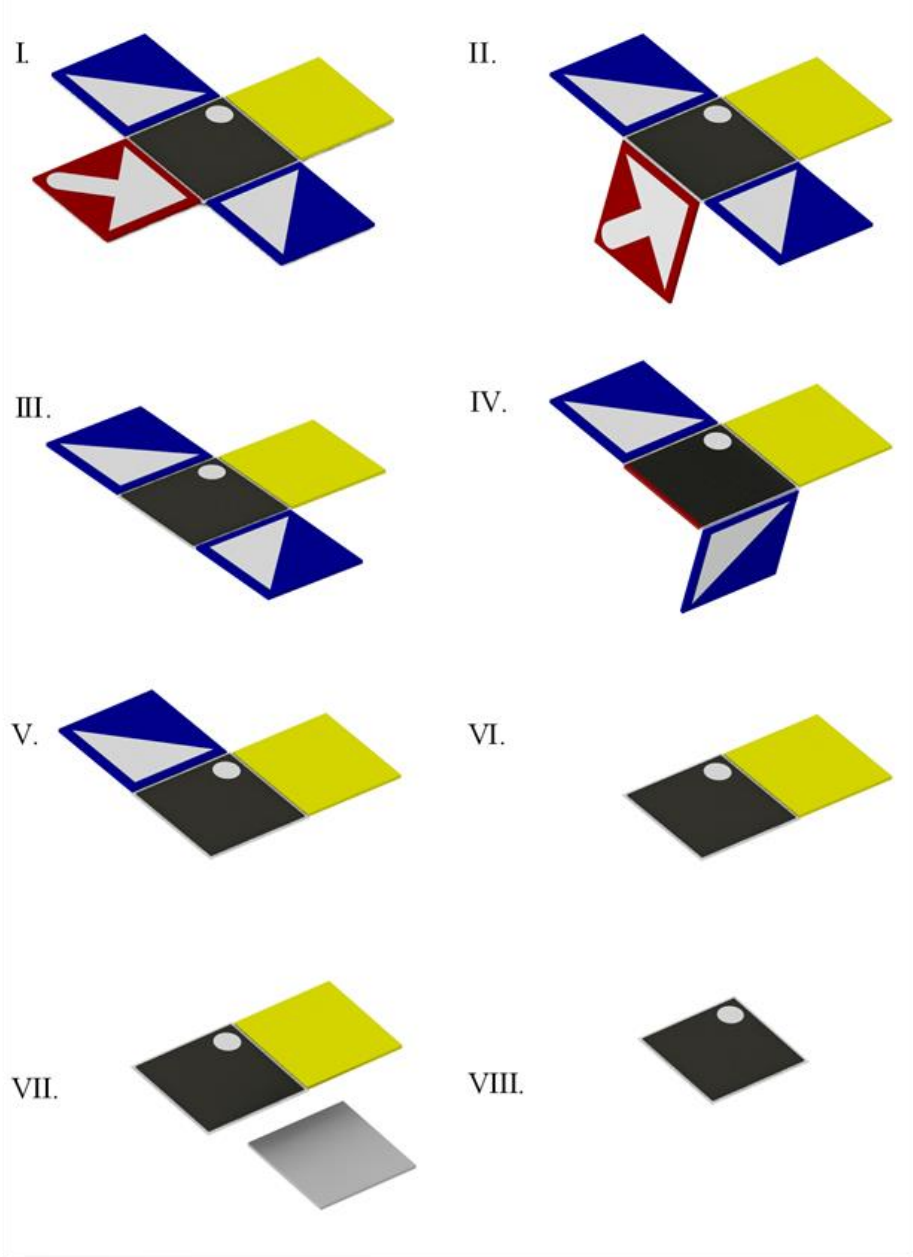

Figure 21. Schematic of paper diagnostic device folding procedures. The folding follows the order of numbers that were labeled in this figure: red, blue, blue, absorbing pad, and yellow (RBBAY). All of the folding are toward to the bottom side of the sampling pad (black).

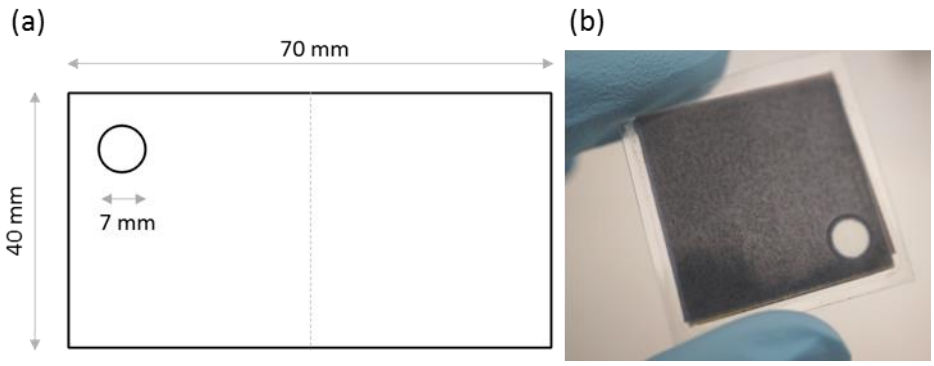

Figure 22. (a) Design of transparent laminate with a length of 70 mm and width of 40 mm, the sampling area opening is a circle with 7 mm in diameter; and (b) the photograph of laminated paper device.

4.2.4. HRP immunoassay optimization

We examined blocking conditions in the paper by adding 5 µl blocking reagents to the sampling area of an assembled paper device and air dried for 20 minutes. The formula of the blocking reagent was 0.1% tween 20, 0.05% SDS, and 1% BSA. The control sample was not treated with any blocking reagent. After 20 minutes, 10 µl 1:2000 diluted anti-*Cryptosporidium*-HRP antibodies (stock concentration is 1 to 2 mg/ml) to both of the paper device incubate for 5 minutes. A total of five repetitive washings were applied after incubation by adding 100 µl PBS buffer each time to both samples. At last, 20 µl TMB were added onto the microspheres for colorimetric reaction. Two devices were then scanned by an Epson (Suwa, Japan) Perfection V500 scanner to observe and record the experiment results.

A series of experiments for optimizing the volume of washing were also examined as following. After blocking, 10 µl 1:2000 diluted anti-*Cryptosporidium*-HRP antibody (stock concentration is 1 to 2 mg/ml) was added to each of the paper devices and incubated for 5 minutes. Different washing protocol were applied across five devices by adding 100

µl PBS for 0, 1, 2, 3, 4, and 5 times respectively. 20 µl TMB were added after for colorimetric reaction. All of the devices were scanned for quantitation as described.

4.2.5. Dose-response with *Cryptosporidium* isolation and detection

The combination of *Cryptosporidium* isolation and paper-based detection were tested. The paper devices were prepared by following the optimized paper fabricating protocol, which was described in section 4.2.4.

The 25-53 µm microspheres were functionalized with protein G and monoclonal anti-*Cryptosporidium* antibodies by following the same protocol described in 4.2.2.1 section. 1 mg of antibody functionalized microspheres were incubated with PBS buffer spiked with 10^2, 10^3, 10^4, and 10^5 *Cryptosporidium* oocysts in 100 µl for two hours. After incubation, 600 µl PBS buffer was added to each sample to form positive meniscus, microspheres carried the captured crypto oocysts float to the top of the meniscus. The microsphere-crypto oocysts complexes were then transferred on to assembled paper-based diagnostic device by touch the sampling area of the device on the meniscus. After the microsphere-crypto complexes were transferred, 10 µl 1:2000 diluted anti-*Cryptosporidium*-HRP antibodies (stock concentration is 1 to 2 mg/ml) were added to the microspheres and incubate for 5 minutes. Unbounded anti-*Cryptosporidium*-HRP antibodies were washed by 100 µl PBS buffer for five times. After the washing, 20 µl TMB were added to each sample and wait for color change. We then took photographs for each sample. The color intensity analysis was done by using Image J software. The Image J color intensity analysis was done by using the circle tool to randomly select 20 spots from each sampling area and measure the mean grey value. The color intensity of each sample

was mean of 20 mean grey value of randomly selected area. The color intensity versus the number of *Cryptosporidium* oocysts spiked were plotted by Microsoft Excel.

4.3 Results

4.3.1. Capture and isolation of *Cryptosporidium* oocysts from buffer and stool

The microsphere separation concept was proofed by *Cryptosporidium* pathogen isolation experiment. The epi-fluorescent imaging in Figure 23a showed the *Cryptosporidium* oocysts were captured by anti-crypto-AF488 antibody and bind with protein G coated microspheres. In contrast, the control sample, showed in Figure 23(b), where the microspheres were not coated with protein G cannot bind with anti-crypto AF488 captured *Cryptosporidium* oocysts. Confocal imaging also confirmed the capturing and isolation of *Cryptosporidium* oocyst by the buoyancy-assisted microspheres in PBS buffer. From the confocal image (Figure 24), we could clearly see two fluorescent crypto oocysts that were pointed by arrow, were captured in between two microspheres. We also found that many of the captured oocysts were sandwiched between two or several microspheres forming a multi-bead complex in both epi-fluorescent and confocal images.

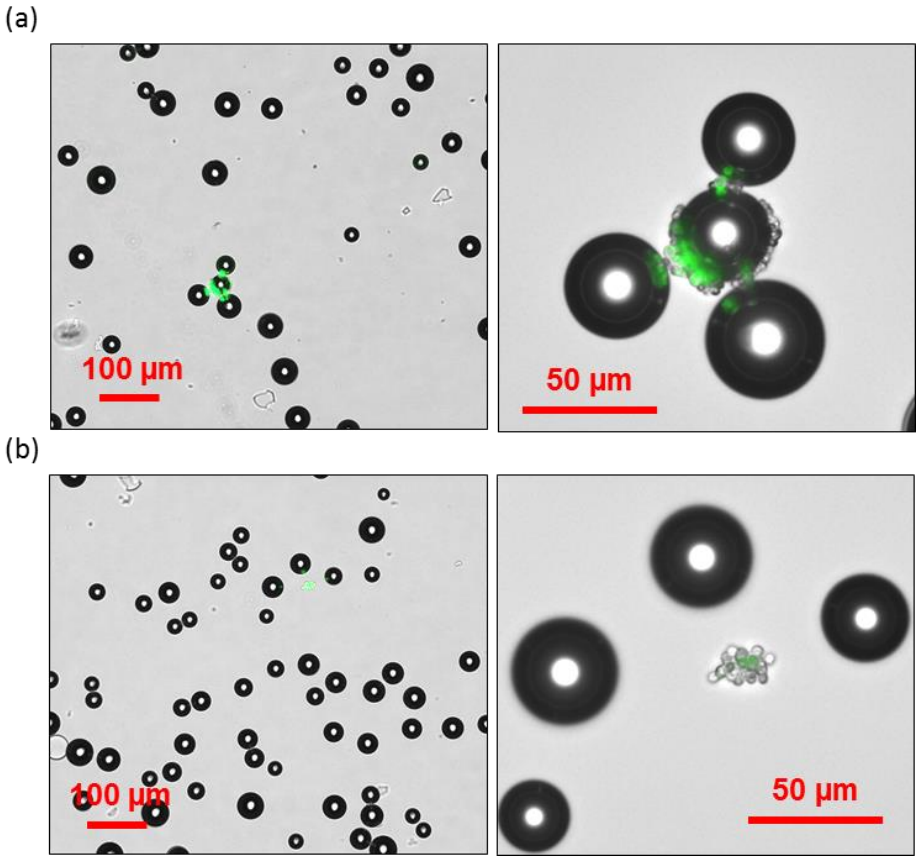

Figure 23. 10x magnitude of the bright-filed and epi-fluorescence overlay images (left), and 40x magnitude (right) for (a) Pre-labeled *Cryptosporidium* oocysts were successfully bound to the protein G-coated molecular buoys, but not the (b) control microspheres.

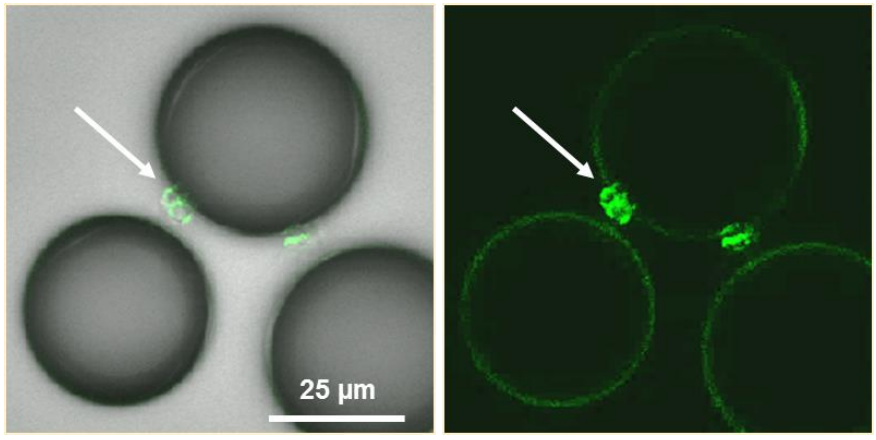

Figure 24. Confocal z-slice image of two *Cryptosporidium* oocysts (white arrow) sandwiched between two hollow silica microspheres in a transmitted light overlay (left) and green fluorescence channel only (right).

The quantity of *Cryptosporidium* oocysts were also analyzed. In order to test the separation efficiency of microspheres, we counted the number of crypto oocysts before they were isolated by microspheres and after the separation in both PBS buffer and stool samples. *Cryptosporidium* oocysts were able to be captured and isolated by using the molecular buoys across a wide range of oocyst concentrations (Figure 25.) in PBS and stool. In general, over 90 % of crypto oocysts were removed by microspheres in both buffer and stool. Negative controls were only blocked by L-cysteine and no protein G coated microspheres, therefore, the anti- *Cryptosporidium* IgGs were not able to be immobilized on the microspheres to actively capture the oocysts. One-tail t-test was applied to analyze the difference between negative control and functionalized microspheres at 10^5 oocysts isolation condition, and the capturing difference between PBS and stool in every category. The t-test result showed that differences between positive and negative samples containing 10^5 oocysts were statistically significant with *p* values of 0.001 in PBS and 0.007 in stool. For the t-test among the stool and PBS, only the 10^5 samples had p value equal to 0.03 which means the number of oocysts captured in stool was slightly lower than buffer. Besides, the standard deviation were low, which indicates the microsphere isolation method has a decent reproducibility.

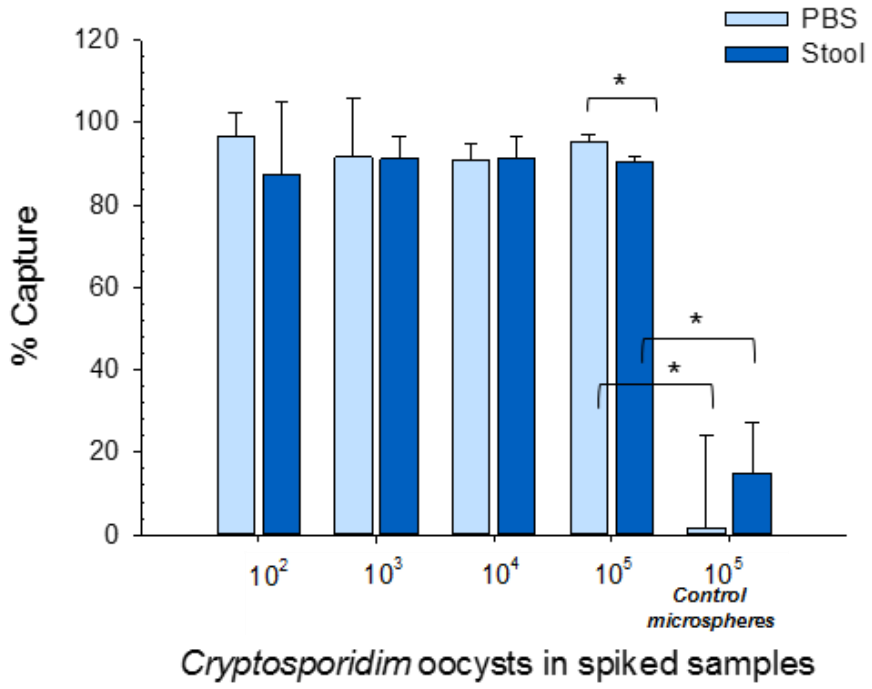

Figure 25. Capture efficiency of the microspheres in buffer and stool samples spiked with different amount of *Cryptosporidium* oocysts. Significant differences using a one-tailed t-test are shown in brackets ($p < 0.05$). The statistical significant differences were found between the control and functionalized microsphere samples, and between the PBS and stool of 10^5 spiked oocysts samples.

4.3.2. HRP immunoassay optimization results

The results of surface blocking test were shown in Figure 26. The paper device without blocking reagent treatment appeared to have a very strong blue color change due to the oxidation of TMB catalyzed by HRP. However, the one with the blocking treatment did not change color, which indicates that the surface blocking process prevented the nonspecific binding of paper efficiently.

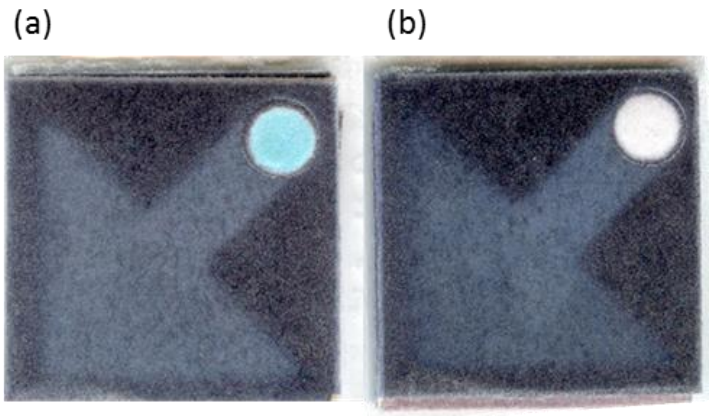

Figure 26. Photographs of a negative control HRP reaction within the paper-microfluidic structure (a) without paper blocking, and (b) with a blocking buffer to reduce non-specific binding.

The results of HRP immunoassay on paper-based devices under different washing buffer volumes were shown in Figure 27. From the results, we could find a progressively decreasing of the blue color with the washing volume increased. However, the background was not eliminated until 5 times of the washing was occurred, which suggested that 5 times of washing is the minimum requirement to rinse off the anti-Crypto-HRP antibody from the sampling area.

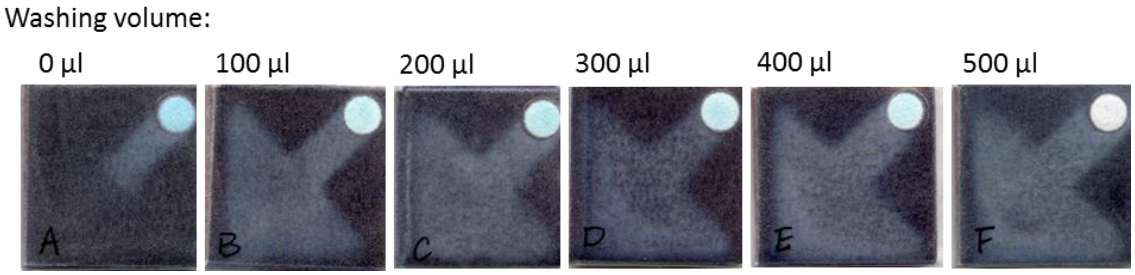

Figure 27. Photographs of paper-based diagnostic devices under different washing conditions, washing volume from left to right: 0, 100, 200, 300, 400, and 500 µl.

4.3.3. Integration of Microsphere Isolation and Detection via Paper-based Device

We integrated the microsphere separation method with our paper-based device technique together. The photographs of each samples were shown in Figure 28a. The blue color intensity was progressively increased due to the amount of *Cryptosporidium* oocysts that were isolated by microspheres were increased. We could also find that the blue color came from the microspheres and the background appeared to be white, which indicated that the oxidization of TMB occurred on the microspheres not from the paper nonspecific binding. The plot of the relationship between color intensity and total crypto amount was shown in Figure 28 (b). The plot demonstrated that the color intensity is dependent upon the amount of *Cryptosporidium* oocysts that isolated by microspheres, and the limit of detection is around 10^4 crypto oocyst/ml.

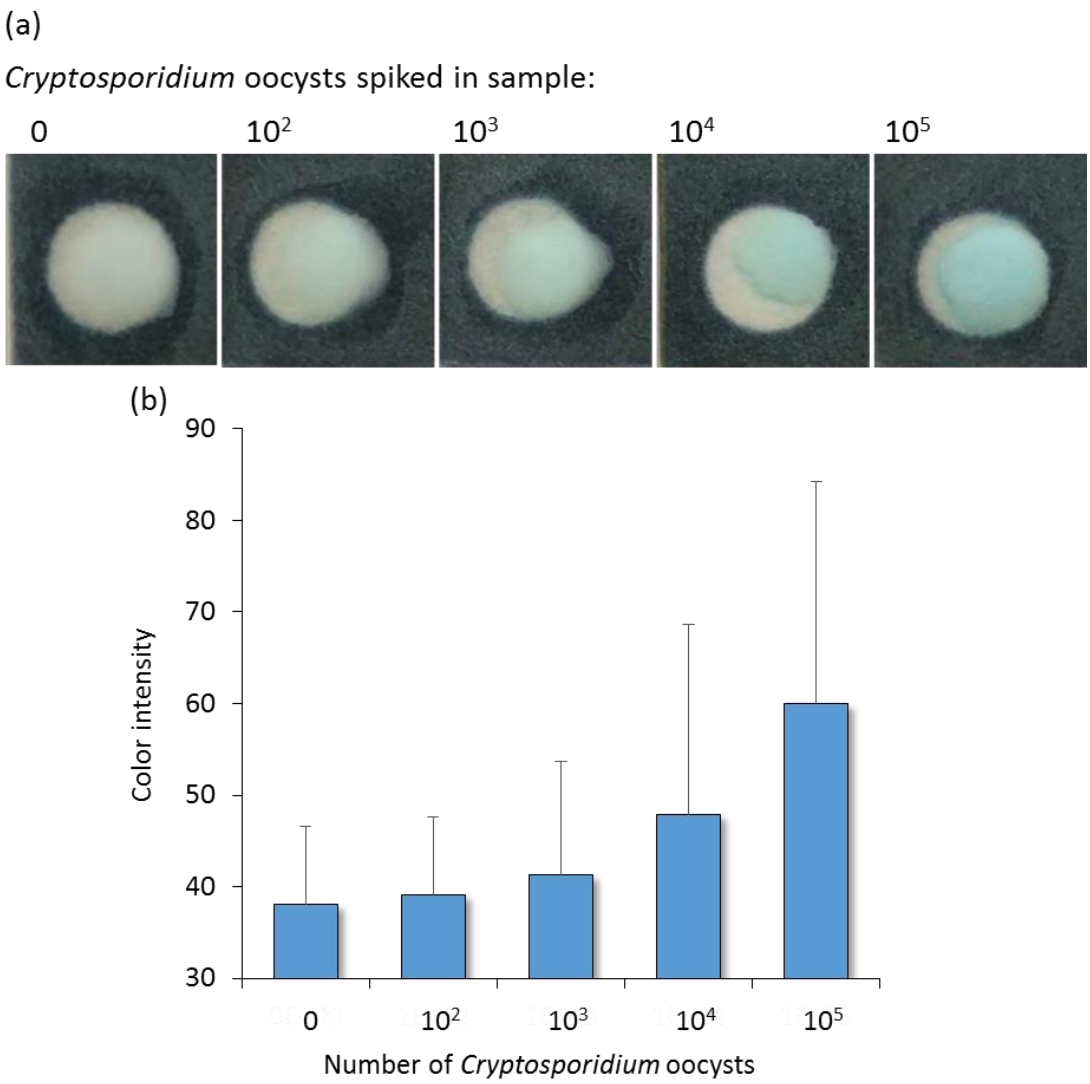

Figure 28. (a) Photographs of microspheres detected on the paper-based diagnostic devices with different amount of *Cryptosporidium* spiked: (left to right) 0, 10^2, 10^3, 10^4, and 10^5, and (b) the color intensity for different amount of *Cryptosporidium*. The error bar represent 3 × σ value.

4.4. Discussions

In the previous chapter, we demonstrated the successful of functionalize the microspheres with target-specific antibodies. In this chapter, the functionalized microspheres were tested to isolate pathogens from both of buffers and the real stool. Both of the epi-fluorescent and the confocal images confirmed that the crypto oocysts were

captured and further isolated by the microspheres. The separation efficiency also quantitatively confirmed that the separation was efficient. Although the separation efficiency results were promising, there were still some problems need to be pointed out. We found that at 10^5 per 100 µl of oocysts condition, the t-test result showed that the separation between stool and PBS has significant difference by the criteria of $p < 0.05$. The reason may due to the disassociation of protein G bound anti-crypto interfered by some biomolecules that existed in the stool. There are also possibilities that the crypto oocysts were hindered or confined by other stool debris, microspheres thus have lower chance to interact with oocysts to capture and isolate them out.

From the previous study of microsphere surface functionalization, we confirmed that the L-cysteine surface blocking performed well, where the negative control samples had nearly no fluorescent signals indicated that the GAM-AF488 antibody could only bind with protein G, but not to the microsphere directly. The remaining problem is the nonspecific binding on the paper. As showed in Figure 26a, paper without treatment with any blocking reagent had a great nonspecific binding problem, and washing with PBS buffer cannot disassociate that binding. The blocked paper device nearly 100% eliminate the nonspecific binding problem by only adding 5 µl of the reagent and following with 5 times of 100 µl PBS washing. We also tested different washing volume for two major reasons: (1) paper device needs be as easy as it could to meet our goal of development of easy to use diagnostic. Too many washing increase the complication of operation. And (2) if the washing is too much, absorbing pad has to be used to hold the liquid volume. Therefore, it adds on the difficulty to assemble and laminate the device. When the device is too thick, it is hard to be laminated, so different layers will not have a close contact.

From the results, we could see the color intensity was progressively decreased when more washes applied, but unfortunately, the background was not disappear until 500 µl PBS was used. A future optimization may be designed to increase the amount of blocking reagent to decrease the washing times and volume.

The color intensity quantification of the paper-based diagnostic device confirmed that the color intensity was dependent upon the amount of *Cryptosporidium* oocysts that isolated by microspheres, which proofed that microsphere separation method are able to integrate with paper-based diagnostic device to provide a pathogen dose dependent diagnose. The colorimetric intensity value of blank sample plus the 3σ was beyond the mean intensity of 10^2 and 10^3, but below the 10^4 samples, which suggested that the limit of detection of this colorimetric assay was at 10^4 level. In order to develop the molecular buoy separation and paper-based diagnostic device as a completely free of use laboratory instrumentation, the colorimetric response signal intensity must be enhanced more. The ultimate goal is to either identify the result virtually even at low pathogen concentration, or quantify the pathogen through smart phone apps by taking photos.

4.5. Conclusions and future directions

This dissertation has demonstrated a successful *Cryptosporidium* pathogen separation method via a hollow centered microsphere, which is a low-cost, instrumentation free, easy to use and efficient alternative separation approach to the existing separation methods. We established the floatation properties of the microspheres, indicate that the microsphere is able to capture and carry the target analyte float to the surface of the solution in a very short time. The separation time is depend on the size and viscosity of the liquid,

and we could control and select the best size of beads into a particular applications. The microspheres are able to functionalize with a variety of biomolecules via an epoxide ring opening reaction, which gives the microsphere a great potential to be used in different applications. This dissertation applied the microsphere separation method in *Cryptosporidium*, a diarrhea pathogen isolation. Both of the microscope images and the quantitation of separation efficiency results confirmed that this microsphere separation method successfully achieve the goal of a low-cost, instrumentation free, easy to use and efficient separation approach.

In addition, a down-stream paper-based diagnostic device was also designed and integrated with the microsphere separation method. The paper-based diagnose device was examined to have a *Cryptosporidium* oocysts dose dependent response, thus successfully integrated with the microsphere separation approach.

In order to fully develop the microsphere separation method and the paper diagnostic device, there are still numbers of tasks need to be tackled, include: (1) The elution of pathogens from microspheres after isolation. (2)The storage period of functionalized microspheres. (3) Protein dissociation rate experiment needs to be done. (4) Optimization of antibody incubation time. (5) Optimization of separation process. (6) How to transfer all of the microspheres to the paper device. (7) Apply the separation method to different pathogen isolations. (8) Enhancement of the colorimetric signal or using other detection methods, such as chemiluminescent assay (9) How to apply the paper detection in mobile phone apps. We believe that with a constant effort on developing and optimizing the microspheres separation method and the paper based diagnostic device will benefit more people and families in the future.

APPENDIX SECTION

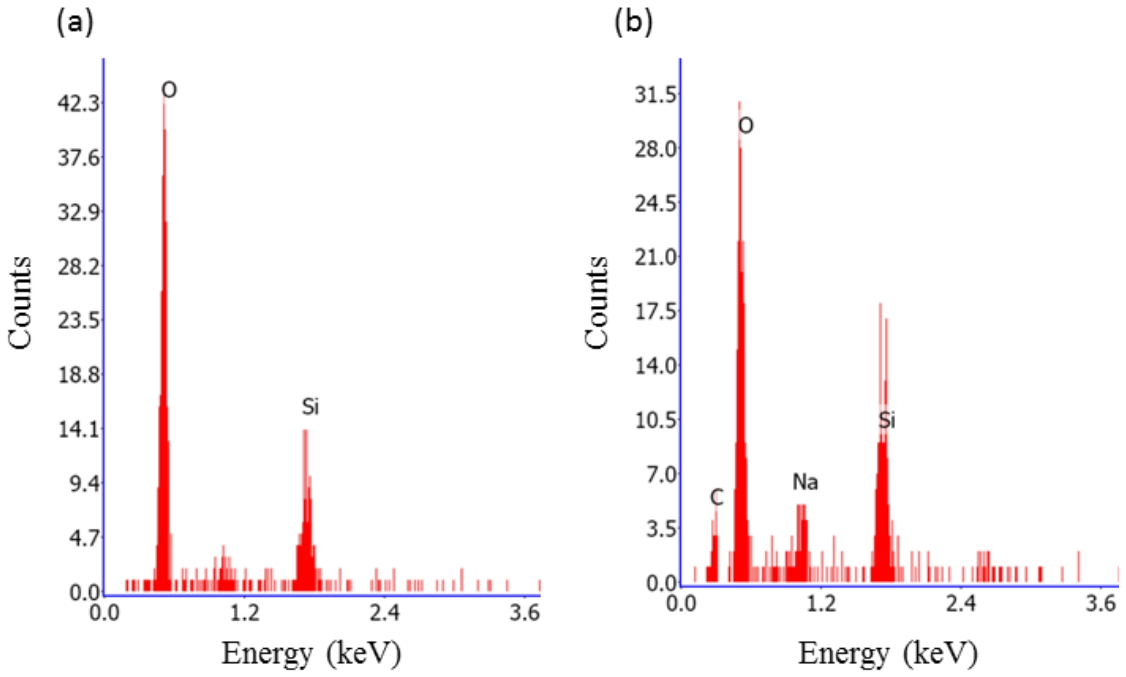

Figure S1. EDAX element analysis for (a) blank microsphere, where only O and Si were found, and (b) Microsphere coated with protein G, where C, O, Na, and Si were found due to the attachment of protein G and buffer salt.

REFERENCES

1. Kalmár, É., et al., *Novel sample preparation method for surfactant containing suppositories: Effect of micelle formation on drug recovery.* Journal of Pharmaceutical and Biomedical Analysis, 2013. **83**: p. 149-156.

2. Zhang, Y., et al., *Microwave Heating in Preparation of Magnetic Molecularly Imprinted Polymer Beads for Trace Triazines Analysis in Complicated Samples.* Analytical Chemistry, 2009. **81**(3): p. 967-976.

3. Saito, Y., et al., *Miniaturized sample preparation needle: A versatile design for the rapid analysis of smoking-related compounds in hair and air samples.* Journal of Pharmaceutical and Biomedical Analysis, 2007. **44**(1): p. 1-7.

4. Pawliszyn, J., *Sampling and sample preparation for field and laboratory: fundamentals and new directions in sample preparation*. Vol. 37. 2002: Elsevier.

5. Hempel, G., *Drug monitoring and clinical chemistry*. Vol. 5. 2004: Elsevier.

6. Wu, J.-T. and D. A.Wells, *Chapter 14 On-line sample preparation: High throughput techniques and strategies for method development*, in *Progress in Pharmaceutical and Biomedical Analysis*, A.W. David, Editor. 2003, Elsevier. p. 505-573.

7. Kataoka, H., *Recent developments and applications of microextraction techniques in drug analysis.* Analytical And Bioanalytical Chemistry, 2010. **396**(1): p. 339-364.

8. Raikos, N., et al., *Analysis of anaesthetics and analgesics in human urine by headspace SPME and GC.* Journal of Separation Science, 2009. **32**(7): p. 1018-1026.

9. Saito, Y., et al., *Direct coupling of microcolumn liquid chromatography with in-tube solid-phase microextraction for the analysis of antidepressant drugs.* Analyst, 2000. **125**(5): p. 807-809.

10. Cutler, P., *Protein purification protocols*. Vol. 244. 2004: Springer Science & Business Media.

11. Yamamoto, S. and E. Miyagawa, *Retention behavior of very large biomolecules in ion-exchange chromatography.* Journal of Chromatography A, 1999. **852**(1): p. 25-30.

12. Englard, S. and S. Seifter, *[22] Precipitation techniques*, in *Methods in Enzymology*, P.D. Murray, Editor. 1990, Academic Press. p. 285-300.

13. Green, A.A. and W.L. Hughes, *[10] Protein fractionation on the basis of solubility in aqueous solutions of salts and organic solvents*, in *Methods in Enzymology*. 1955, Academic Press. p. 67-90.

14. Yamamoto, S. and T. Ishihara, *Ion-exchange chromatography of proteins near the isoelectric points.* Journal of Chromatography A, 1999. **852**(1): p. 31-36.

15. Sluyterman, L. and O. Elgersma, *Chromatofocusing: Isoelectric focusing on ion-exchange columns: I. General Principles.* Journal of Chromatography A, 1978. **150**(1): p. 17-30.

16. Righetti, P.G., *Isoelectric focusing: theory, methodology and applications*. Vol. 299. 1983: Elsevier Biomedical Press Amsterdam.

17. Burnouf, T., *Chromatography in plasma fractionation: benefits and future trends.* Journal of Chromatography B: Biomedical Sciences and Applications, 1995. **664**(1): p. 3-15.

18. Katakam, M. and A.K. Banga, *Aggregation of insulin and its prevention by carbohydrate excipients.* PDA Journal of Pharmaceutical Science and Technology, 1995. **49**(4): p. 160-165.

19. Irvine, G.B., *High-performance size-exclusion chromatography of peptides.* Journal of biochemical and biophysical methods, 2003. **56**(1): p. 233-242.

20. Wen, J., T. Arakawa, and J.S. Philo, *Size-exclusion chromatography with on-line light-scattering, absorbance, and refractive index detectors for studying proteins and their interactions.* Analytical biochemistry, 1996. **240**(2): p. 155-166.

21. Hammond, G., et al., *Estimation of the percentage of free steroid in undiluted serum by centrifugal ultrafiltration-dialysis.* Journal of Biological Chemistry, 1980. **255**(11): p. 5023-5026.

22. Cheryan, M., *Ultrafiltration handbook*. 1986: Technomic Publishing Co. Inc.

23. Cheryan, M., *Ultrafiltration and microfiltration handbook*. 1998: CRC press.

24. Slingeneyer, A., B. Canaud, and C. Mion, *Permanent loss of ultrafiltration capacity of the peritoneum in long-term peritoneal dialysis: an epidemiological study*. Nephron, 1983. **33**(2): p. 133-138.

25. Porath, J., *Strategy for Differential Protein Affinity Chromatrography*. IJBC, 2001. **6**(1): p. 51-78.

26. Urh, M., D. Simpson, and K. Zhao, *Affinity chromatography: general methods.* Methods in enzymology, 2009. **463**: p. 417-438.

27. Clonis, Y., et al., *Biomimetic dyes as affinity chromatography tools in enzyme purification.* Journal of Chromatography A, 2000. **891**(1): p. 33-44.

28. Hill, C., A. Kenney, and L. Goulding. *The design, development and use of immunopurification reagents*. in *Biotech. Forum*. 1987.

29. Dunbar, B.S. and E.D. Schwoebel, *Preparation of polyclonal antibodies.* Methods in enzymology, 1990. **182**: p. 663.

30. Köhler, G. and C. Milstein, *Continuous cultures of fused cells secreting antibody of predefined specificity.* nature, 1975. **256**(5517): p. 495-497.

31. Schmitt, J., H. Hess, and H.G. Stunnenberg, *Affinity purification of histidine-tagged proteins.* Molecular biology reports, 1993. **18**(3): p. 223-230.

32. Skerra, A. and T.G. Schmidt, *Applications of a peptide ligand for streptavidin: the Strep-tag.* Biomolecular engineering, 1999. **16**(1): p. 79-86.

33. Gaberc-Porekar, V. and V. Menart, *Perspectives of immobilized-metal affinity chromatography.* Journal of biochemical and biophysical methods, 2001. **49**(1): p. 335-360.

34. Yarmush, M.L., et al., *Immunoadsorption: strategies for antigen elution and production of reusable adsorbents.* Biotechnology progress, 1992. **8**(3): p. 168-178.

35. He, J., et al., *Magnetic separation techniques in sample preparation for biological analysis: A review.* Journal of Pharmaceutical and Biomedical Analysis, 2014. **101**: p. 84-101.

36. Li, Y., X. Zhang, and C. Deng, *Functionalized magnetic nanoparticles for sample preparation in proteomics and peptidomics analysis.* Chemical Society Reviews, 2013. **42**(21): p. 8517-8539.

37. Shao, D., et al., *Polyaniline multiwalled carbon nanotube magnetic composite prepared by plasma-induced graft technique and its application for removal of aniline and phenol.* The Journal of Physical Chemistry C, 2010. **114**(49): p. 21524-21530.

38. Toh, P.Y., et al., *Magnetophoretic removal of microalgae from fishpond water: feasibility of high gradient and low gradient magnetic separation.* Chemical Engineering Journal, 2012. **211**: p. 22-30.

39. Jonker, N., et al., *Online magnetic bead dynamic protein-affinity selection coupled to LC− MS for the screening of pharmacologically active compounds.* Analytical Chemistry, 2009. **81**(11): p. 4263-4270.

40. Xu, N., et al., *High-Performance Liquid Chromatography–Electrospray Ionization-Mass Spectrometry Ligand Fishing Assay: A Method for Screening Triplex DNA Binders from Natural Plant Extracts.* Analytical Chemistry, 2012. **84**(5): p. 2562-2568.

41. Tao, Y., et al., *Rapid screening and identification of α-glucosidase inhibitors from mulberry leaves using enzyme-immobilized magnetic beads coupled with HPLC/MS and NMR.* Biomedical Chromatography, 2013. **27**(2): p. 148-155.

42. Shao, M., et al., *Preparation of Fe3O4@ SiO2@ layered double hydroxide core–shell microspheres for magnetic separation of proteins.* Journal of the American Chemical Society, 2012. **134**(2): p. 1071-1077.

43. Hu, X., et al., *Preparation and evaluation of solid-phase microextraction fiber based on molecularly imprinted polymers for trace analysis of tetracyclines in complicated samples.* Journal of Chromatography A, 2008. **1188**(2): p. 97-107.

44. Zhang, X., et al., *Preparation of Fe3O4@ C@ layered double hydroxide composite for magnetic separation of uranium.* Industrial & Engineering Chemistry Research, 2013. **52**(30): p. 10152-10159.

45. Didar, T.F. and M. Tabrizian, *Adhesion based detection, sorting and enrichment of cells in microfluidic Lab-on-Chip devices.* Lab on a Chip, 2010. **10**(22): p. 3043-3053.

46. Bonner, W., et al., *Fluorescence activated cell sorting.* Review of Scientific Instruments, 1972. **43**(3): p. 404-409.

47. Gänshirt-Ahlert, D., et al., *Magnetic cell sorting and the transferrin receptor as potential means of prenatal diagnosis from maternal blood.* American journal of obstetrics and gynecology, 1992. **166**(5): p. 1350-1355.

48. Plouffe, B.D. and S.K. Murthy, *Perspective on microfluidic cell separation: a solved problem?* Analytical Chemistry, 2014. **86**(23): p. 11481-11488.

49. Manz, A., et al., *Planar chips technology for miniaturization and integration of separation techniques into monitoring systems: capillary electrophoresis on a chip.* Journal of Chromatography A, 1992. **593**(1): p. 253-258.

50. Whitesides, G.M., *The origins and the future of microfluidics.* nature, 2006. **442**(7101): p. 368-373.

51. Alix-Panabières, C., H. Schwarzenbach, and K. Pantel, *Circulating tumor cells and circulating tumor DNA.* Annual review of medicine, 2012. **63**: p. 199-215.

52. Bhagat, A.A.S., et al., *Microfluidics for cell separation.* Medical & biological engineering & computing, 2010. **48**(10): p. 999-1014.

53. Di Carlo, D., *Inertial microfluidics.* Lab on a Chip, 2009. **9**(21): p. 3038-3046.

54. Matas, J.-P., J.F. Morris, and É. Guazzelli, *Inertial migration of rigid spherical particles in Poiseuille flow.* Journal of Fluid Mechanics, 2004. **515**: p. 171-195.

55. Zhang, J., et al., *Fundamentals and applications of inertial microfluidics: a review.* Lab on a Chip, 2016. **16**(1): p. 10-34.

56. Davis, J.A., et al., *Deterministic hydrodynamics: taking blood apart.* Proceedings of the National Academy of Sciences, 2006. **103**(40): p. 14779-14784.

57. Liou, Y.-R., et al., *Buoyancy-Activated Cell Sorting Using Targeted Biotinylated Albumin Microbubbles.* PloS one, 2015. **10**(5): p. e0125036.

58. Song, J., et al., *Label-free density difference amplification-based cell sorting.* Biomicrofluidics, 2014. **8**(6): p. 064108.

59. Hsu, C., et al. *Isolating cells from blood using buoyancy activated cell sorting (BACS) with glass microbubbles*. in *14th International Conference on Miniaturized Systems for Chemistry and Life Sciences*. 2010.

60. Shi, G., et al., *Isolation of rare tumor cells from blood cells with buoyant immuno-microbubbles.* PloS one, 2013. **8**(3): p. e58017.

61. Simberg, D. and R. Mattrey, *Targeting of perfluorocarbon microbubbles to selective populations of circulating blood cells.* Journal of drug targeting, 2009. **17**(5): p. 392-398.

62. Perry, J.L., J.S. Matthews, and G.R. Miller, *Parasite detection efficiencies of five stool concentration systems.* J Clin Microbiol, 1990. **28**(6): p. 1094-7.

63. Dryden, M.W., et al., *Gastrointestinal Parasites: The Practice Guide to Accurate Diagnosis and Treatment.* Suppl Compend Contin Educ Vet, 2006. **28**(8A).

64. White, A.C., *Cryptosporidiosis (Cryptosporidium hominis, Cryptosporidium parvum and Other species)*, in *Principles and Practice of Infectious Diseases*, Mandell, Bennett, and Dolin, Editors. 2010, Churchill Livingstone. p. 3547-3560.

65. Hermanson, G.T., *Bioconjugate techniques.* 1996, San Diego: Academic Press. xxv, 785 p.

66. Schneider, C.A., W.S. Rasband, and K.W. Eliceiri, *NIH Image to ImageJ: 25 years of image analysis.* Nat Methods, 2012. **9**(7): p. 671-5.

67. Boron, W.F. and E.L. Boulpaep, *Medical Physiology*. 2016: Elsevier Health Sciences.

68. Segur, J.B. and H.E. Oberstar, *Viscosity of Glycerol and Its Aqueous Solutions.* Industrial & Engineering Chemistry, 1951. **43**(9): p. 2117-2120.

69. Bosart, L.W. and A. Snoddy, *Specific gravity of glycerol.* Industrial and Engineering Chemistry, 1928. **20**(1): p. 1377-1379.

70. Batchelor, G.K., *An Introduction to Fluid Dynamics*. Cambridge Mathematical Library. Vol. 2nd pbk. ed. 1999, Cambridge, U.K.: Cambridge University Press.

71. Dawson, R.M.C., *Data for biochemical research*. 3rd ed. 1986, Oxford: Clarendon Press. xii, 580 p.

72. Kato, K., et al., *Model for the complex between protein G and an antibody Fc fragment in solution.* Structure, 1995. **3**(1): p. 79-85.

73. Lynch, I. and K.A. Dawson, *Protein-nanoparticle interactions.* Nano today, 2008. **3**(1): p. 40-47.

74. Iqbal, A., et al., *Detection of Cryptosporidium parvum Oocysts on Fresh Produce Using DNA Aptamers.* PloS one, 2015. **10**(9): p. e0137455.

75. Richards-Kortum, R. *Point-of-Care Diagnostics for Low-Resource Settings*. in *Frontiers in Optics*. 2014: Optical Society of America.

76. Peeling, R.W., et al., *Rapid tests for sexually transmitted infections (STIs): the way forward.* Sexually transmitted infections, 2006. **82**(suppl 5): p. v1-v6.

77. Clegg, D.L., *Paper chromatography.* Analytical Chemistry, 1950. **22**(1): p. 48-59.

78. Qureshi, S.Z., S.T. Ahmad, and S. Haque, *Filter-paper test for microgram detection of aliphatic amines.* Talanta, 1990. **37**(7): p. 763-765.

79. Comer, J., *Semiquantitative specific test paper for glucose in urine.* Analytical Chemistry, 1956. **28**(11): p. 1748-1750.

80. Rorem, E.S. and J. Lewis, *A test paper for the detection of galactose and certain galactose-containing sugars.* Analytical biochemistry, 1962. **3**(3): p. 230-235.

81. Singer, J.M. and C.M. Plotz, *The latex fixation test: I. Application to the serologic diagnosis of rheumatoid arthritis.* The American journal of medicine, 1956. **21**(6): p. 888-892.

82. O'Farrell, B., *Lateral Flow Immunoassay Systems: 2.4 Evolution from the Current State of the Art to the Next Generation of Highly Sensitive, Quantitative Rapid Assays.* The Immunoassay Handbook: Theory and applications of ligand binding, ELISA and related techniques, 2013: p. 89.

83. O'Farrell, B., *Evolution in lateral flow–based immunoassay systems*, in *Lateral Flow Immunoassay*. 2009, Springer. p. 1-33.

84. Posthuma-Trumpie, G.A., J. Korf, and A. van Amerongen, *Lateral flow (immuno) assay: its strengths, weaknesses, opportunities and threats. A literature survey.* Analytical And Bioanalytical Chemistry, 2009. **393**(2): p. 569-582.

85. Sajid, M., A.-N. Kawde, and M. Daud, *Designs, formats and applications of lateral flow assay: A literature review.* Journal of Saudi Chemical Society, 2015. **19**(6): p. 689-705.

86. Martinez, A.W., et al., *Patterned paper as a platform for inexpensive, low‐volume, portable bioassays.* Angewandte Chemie International Edition, 2007. **46**(8): p. 1318-1320.

87. Martinez, A.W., et al., *FLASH: a rapid method for prototyping paper-based microfluidic devices.* Lab on a Chip, 2008. **8**(12): p. 2146-2150.

88. Carrilho, E., A.W. Martinez, and G.M. Whitesides, *Understanding wax printing: a simple micropatterning process for paper-based microfluidics.* Analytical Chemistry, 2009. **81**(16): p. 7091-7095.

89. Martinez, A.W., et al., *Diagnostics for the developing world: microfluidic paper-based analytical devices.* Analytical Chemistry, 2009. **82**(1): p. 3-10.

90. Martinez, A.W., S.T. Phillips, and G.M. Whitesides, *Three-dimensional microfluidic devices fabricated in layered paper and tape.* Proceedings of the National Academy of Sciences, 2008. **105**(50): p. 19606-19611.